Effects of a *Mycobacterium smegmatis*-related Strain on the Inflammatory Signaling of BV-2 Murine Microglia Assessed via the NanoString Platform

By

William J. Sanders

Undergraduate Thesis – University of Colorado Boulder

Department of Molecular, Cellular & Developmental Biology

Committee Members:

Thesis Advisor – Dr. Christopher A. Lowry; Integrative Physiology

Honors Council Representative – Dr. Christy Fillman; Molecular, Cellular & Developmental Biology

Outside Reader – Dr. Teresa Foley; Integrative Physiology

Friday April 7th, 2023, at 12:00 PM

Acknowledgements

Special thanks to Dr. Christopher A. Lowry, Dr. Cristian A. Zambrano, Dr. Rolf Norgaard, Evan M. Holbrook, Luke W. Desmond, Caelan T.O. Wright, Lamya'a M. Dawud, the Behavioral Neuroendocrinology Lab, the Department of Integrative Physiology, the Department of Molecular, Cellular & Developmental Biology, the Undergraduate Research Opportunities Program, and Jeremy T. Rahkola of the Rocky Mountain Regional Veterans Affairs Medical Center (RMRVAMC) for their assistance on this project. Murine BV-2 cells were a generous gift from Dennis J. Selkoe, Brigham Women's, Cambridge, MA.

Table of Contents

Abstract

Individuals residing in high-income, industrialized countries are facing higher rates of inflammatory disease and stress-linked psychiatric disorders for which inflammation is a risk factor. The "Old Friends" Hypothesis asserts that this trend exists in part due to reduced exposure to commensal microorganisms (Rook et al., 2013). *Mycobacterium vaccae* NCTC 11659, a strain of soil-derived and non-pathogenic bacterium, has been shown to attenuate inflammation and stress-linked behavior in murine studies (Reber et al., 2016). Analyzing the effects of related bacterial strains on immune tissue provides information on the yet undiscovered molecular mechanisms at play and can help determine which species have the strongest immunoregulatory effects.

This experiment investigates the effects of a yet unnamed species of *Mycobacterium*, closely related to *M. vaccae* and *M. smegmatis*, on BV-2 murine microglia. Microglia, which reside in the central nervous system, are not typically exposed to bacteria and must be able to defend neural tissue when necessary. Due to their functional niche, the BV-2 cells are expected to exhibit a pro-inflammatory response after bacterial contact, along with possible strain-specific responses (Loane & Byrnes, 2010). Cultured BV-2 cells were divided into 12 samples (three replicates of four conditions) and each condition received doses of an inflammatory agent (lipopolysaccharide, LPS), the novel mycobacterial strain, and/or growth media. Extraction of mRNA using Qiagen RNeasy kits permitted NanoString transcript sequencing, where relative levels of mRNA transcripts are measured and compared. Although one replicate in the LPS + *M. smegmatis*-related strain group could not be included in statistical analysis, the data do not indicate any strong immunomodulatory effects from treatment with the novel strain, and instead suggest that it generates a mild inflammatory phenotype in microglia.

Introduction

Many illnesses are affected by, or even propagated through, the body's pro-inflammatory signaling pathways. Injuries and infections generally induce inflammation, as this response evolved as a means to promote the defense, healing, and restoration of tissues (Doolittle, 2011). The human immune response can be divided into two main pathways: the innate and adaptive immune systems. Cells such as macrophages, dendritic cells, and microglia make up the innate immune system and are the body's initial response to the introduction of a pathogen. They react quickly to the presence of foreign material by causing inflammation, attacking intruding microorganisms, and communicating with adaptive immune cells via the release of cytokines. Murine microglia, which are modeled in this experiment using BV-2 cells, form part of the central nervous system tissues and account for between 5% and 12% of cells in different areas of the brain and spinal cord. Microglia are most concentrated in the substantia nigra, a dopaminergic center, basal ganglia, and hippocampus. These regions control core bodily and mental functions, such as movement, reward sensation, and memory (Lawson et al., 1990).

The adaptive immune response activates more slowly than the innate immune response and is incredibly specific. B- and helper T-lymphocytes are activated via the innate immune response and release pathogen-specific antibodies, which recruit killer T-lymphocytes. Additionally, the specificity of T-cell receptors allows them to explicitly target antigen presented to them by other leukocytes (Hoebe et al., 2004). Regulatory T-cells (Tregs), typically FoxP3+ leukocytes, are generally antagonistic towards other cells' immune responses and rely on interleukin-10 (IL-10) to quell inflammation and induce Tr1-type (FoxP3-) Tregs. Underpopulated and/or ineffective Tregs are thought to influence many chronic inflammatory conditions (Grazia Roncarolo et al., 2006). Microglia can also interact with and prime T-cells via chemical signaling. Microglial

misregulation of T-cell function, especially when through the over-expression of major histocompatibility complex II (MHC-II) has been linked to neurodegeneration and excess inflammation (Schetters et al., 2018).

The molecules released during episodes of inflammation differ. Some cytokines, such as IL-1β, tumor necrosis factor-α (TNF-α), and complement proteins, are characteristic of acute inflammatory responses. Chronic inflammation can involve these and numerous other compounds (Furman et al., 2019). These cytokines drive inflammation, recruit leukocytes, and propagate the immune response. When inflammatory pathways become over-activated, the body may interpret stimuli incorrectly and harm itself. Autoimmune disorders, such as arthritis and insulin-dependent diabetes mellitus, cause immune cells to recognize healthy tissues as pathogenic and attack them (Kany et al., 2019).

Increased release of inflammatory cytokines appears to trigger so-called "sickness behaviors," such as "sadness, anhedonia, fatigue, reduced libido and food intake, altered sleep and social-behavioral withdrawal, as well as increased blood pressure, insulin resistance and dyslipidemia." Although they evolved to promote energy conservation while combatting illnesses, many of these traits are considered key symptoms of disorders namely, depression, anxiety, and post-traumatic stress disorder (Furman et al., 2019). Although we do not fully understand the mechanisms that determine individuals' risk of stress-induced anxiety and stress-related psychiatric disorders, evidence suggests that exaggerated pro-inflammatory responses may play a significant role (Pace et al., 2006).

In many areas, incidence of inflammation-related disease skyrocketed during and after industrialization, while rates of infectious disease have fallen (Ehlers & Kaufmann, 2010).

As societies industrialize, their populations tend to urbanize, and individuals spend more time inside. The "Old Friends" hypothesis posits that decreased contact with commensal environmental microorganisms, especially early in life, can lead to the misregulation of immune responses (Rook et al., 2013). In a German study, individuals who grew up in cities with populations greater than 100,000 and without daily exposure to pets responded differently to psychosocial stressors. After completing the Trier social stress test (TSST), these individuals experienced heightened numbers of circulating peripheral blood mononuclear cells (PBMCs) and increased levels of the pro-inflammatory cytokine interleukin 6 (Böbel et al., 2018). This is similar to the heightened interleukin 6 responses seen in individuals diagnosed with major depressive disorder after performing the TSST (Pace et al., 2006). Inflammation-related ailments degrade the quality of life of millions of people around the globe, and a better understanding of pro-inflammatory pathways along with new methods of combatting excess inflammation could greatly improve multitudes of lives (Ouabbou et al., 2020).

With this hypothesis in mind, it is easy to associate the lifestyle of industrial societies with increased rates of inflammatory disorders among their populations. An example of a commensal "old friend" derived from soil is *Mycobacterium vaccae* NCTC 11659. Exposure to this bacterial species has been shown to downregulate pro-inflammatory genes in immune cells derived from human and murine hosts (Zuany-Amorim et al., 2002). *In vivo* murine models also exhibited increased behavioral resilience to stressors post-exposure (Reber et al., 2016). While the immunoregulatory effects of *M. vaccae* have been observed, the molecular mechanisms by which they are achieved remains unknown. Multiple patterns of interaction between "old friends" and immunoregulatory cells have been proposed. They are classed as either "direct," where microbiota directly secrete molecules that modulate host immunoregulation, or "indirect",

where “old friends” modulate a relationship between the host and other microorganisms, like gut biota (Rook et al., 2013).

This project investigates the effects of a novel strain of bacteria on the inflammatory signaling pathways of murine BV-2 microglia. This new strain remains unnamed but is closely related to *M. vaccae* NCTC 11659 and another soil-derived bacterium, *M. smegmatis*. All mycobacteria are related to *M. tuberculosis*, which uses its anti-inflammatory properties to avoid immune detection (Józefowski et al., 2008). Some mycobacteria, like *M. vaccae* NCTC 11659*,* demonstrate similar immunoregulatory effects, yet are not considered pathogenic (Sweeney et al., 2011). As the novel strain is closely related to these species, it is likely to demonstrate similar properties and remains an important candidate for study. *M. smegmatis* has not been shown to induce the same immunoregulatory effects as *M. vaccae* NCTC 11659 and is known to have formed colonies on human skin (Wallace et al., 1988). Exposure to some recombinant strains of *M. smegmatis* has conferred strong immunity against *M. tuberculosis* infections, indicating that similar proteins may be expressed on the exterior of both species (Sweeney et al., 2011). This novel strain was provided by the Behavioral Neuroendocrinology Laboratory (University of Colorado Boulder, Boulder, CO).

Microglia are the immune cells responsible for regulating inflammation and synaptic pruning in neural tissue (Loane & Byrnes, 2010). BV-2 cells are microglia originating from the C57BL/6 strain of mice that have been immortalized via a v-raf/v-myc carrying J2 retrovirus (Henn, 2009). Understanding how they react to the novel bacteria could shed light onto the mechanisms by which related strains lower levels of neural inflammation. As the innate immune system reacts quickly and serves as a recruiter of adaptive immune cells, cells from innate lineages are more

accurate models for initial environmental exposure to microorganisms. Due to their location in nervous tissue, these cells rarely encounter pathogens. As they are highly specified for this environment, the microglia are expected to exhibit an inflammatory response after exposure to any bacteria, as well as possible responses characteristic of the novel strain.

To determine how these bacteria affect BV-2 microglia, trial groups will be exposed to a heat-killed preparation of the *Mycobacterium*, lipopolysaccharide (an inflammatory agent), both, or neither. Afterwards, the mRNA content of the cells will be analyzed using the NanoString Sprint and Rosalind analysis platforms. This research serves as a base for the further development of mycobacteria-based treatments for inflammation-related disorders. As the rates of diseases associated with inflammation continue to rise, it is important that new, more effective therapeutics are derived and that the root causes of these conditions are understood.

Materials and Methods

BV-2 murine microglial cells

BV-2 microglial cells are a standard immortalized C57BL/6 murine cell line that has been infected with *v-raf/ v-myc* oncogene carrying retrovirus (J2) (Blasi et al., 1990). BV-2 cells were obtained from Dennis J. Selkoe (Brigham Women's, Cambridge, MA) on September 14, 2020 and cultured in DMEM/F12 (Cat. No. 12634-010, Gibco-Invitrogen, ThermoFisher Scientific, Waltham, MA) medium supplemented with 10% fetal bovine serum (FBS; Hyclone; Cat. No. F9423, Sigma-Aldrich, Saint Louis, MO, USA) and 1% penicillin/streptomycin (100 U/ml penicillin and 100 µg/ml streptomycin; Cat. No. 15140-122, Gibco, Waltham, MA, USA) under standard culture conditions (37 ºC in a humidified 5% CO_2 incubator). The cells grew on 24-well VWR tissue culture plates, sterile surface (Cat. No. 10062-896, VWR North America, Radnor,

PA). After plating, each well contained 200,000 BV-2 cells in 0.5 mL of media. To harvest BV-2 cells, cells were trypsinized (0.25% trypsin/EDTA; Cat No. 25200-056, Gibco, Waltham, MA), then centrifuged (500 rpm for 5 min at 21-23 °C) and resuspended in fresh DMEM/F12 medium.

Experimental timeline

The experimental timeline is illustrated in Fig. 1. BV-2 plating occurred at hour 0. Each well contained 200,000 BV-2 cells in 0.5 mL of DMEM/F12 medium supplemented with 10% FBS and 1% penicillin/streptomycin under standard culture conditions (37 °C and 5% CO2 in a humidified incubator). At hour 24, 6 wells (1-3, 7-9) received 15 µL of 3.33 mg/mL of the novel bacterial strain and the 6 other wells (4-6, 10-12) 15 µL of borate-buffered saline (BBS), the vehicle solution containing the bacteria, as a control. At hour 48, we stimulated three of the *Mycobacterium*-treated wells and three of the BBS-treated wells with LPS (E. *coli* O111:B4 lipopolysaccharide, Cat. No. L2630, Sigma-Aldrich) until reaching a concentration of 0.250 µg/ml in each well. At hour 72, mRNA purification and collection were performed using RNeasy Mini kits (Cat. No. 74104, QIAGEN, Hilden, Germany). Nanodrop analysis (Cat. No. ND-ONE-W, ThermoFisher Scientific, Madison, WI, USA) then confirmed the RNA concentration was 5 ng/µl in each sample. Samples were then sent to the Core Equipment Facility at the Veterans Health Administration, Rocky Mountain Regional Veterans Affairs Medical Center (RMRVAMC) for analysis of mRNA expression using the NanoString nCounter Sprint system.

Figure 1: Experimental Timeline and Design

A. Timeline

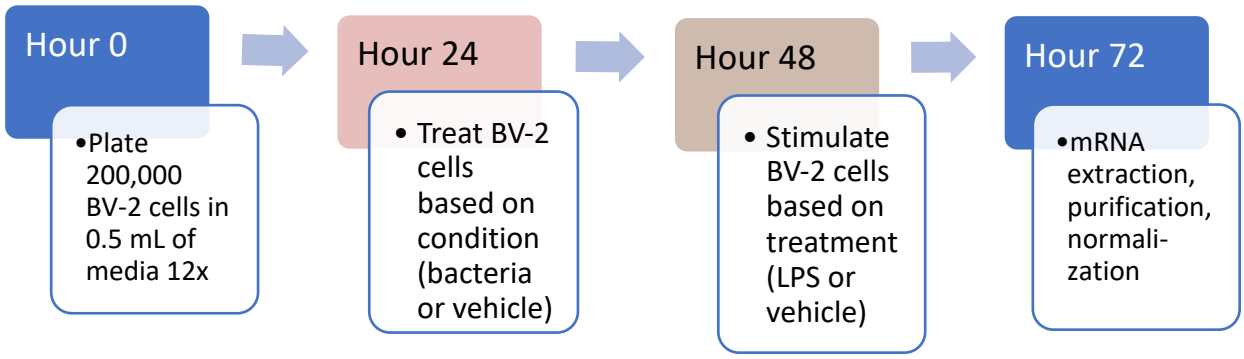

B. Experimental Design

Treatment Group Structure	**Vehicle (BBS)**	**LPS + vehicle**
Vehicle	Vehicle (BBS) group	LPS + BBS group
***M. smegmatis*-like strain + vehicle**	Myco + BBS group	LPS + Myco group

* = hour 24, = hour 48

**One sample in the LPS + Myco group was flagged for quality control and excluded from analysis. This sample is marked with X.

RNA Extraction

RNA was extracted from the BV-2 cells using QIAGEN RNeasy Mini Plus kits (Cat. No. 74104, QIAGEN, Hilden, Germany). This procedure was performed according to the provided instructions in six steps (below), 24 hours after treating the cells with 250 ng/mL LPS (*E. coli* O111:B4) or vehicle (BBS).

1. Lysing BV-2s. In each well, the recommended 350 µl of RLT buffer provided in the RNeasy Mini Plus kit was added to the BV-2 cells, followed by the given volume of 70% ethanol to the lysate. The solution was mixed thoroughly with a pipette.
2. Up to 700 µl of sample, including any precipitate, was transferred to an RNeasy Mini spin filter column placed in a provided 2 ml collection tube. The samples were then centrifuged for 15 seconds at 8000G. The centrifuge separated the contents of the mixture, allowing for the collection of mRNA and the disposal of liquid waste.
3. 700 µl of the RWQ buffer was added to each of the RNeasy spin columns. The samples were then centrifuged for 15 seconds at 8000G, and the flow-through was discarded.
4. 500 µl of RPE buffer was added to the RNeasy spin column. The flow-through was discarded after centrifuging for 15 seconds at 8000G.
5. Identical procedure to step 4, except that the centrifuge duration was increased from 15 to 120 seconds.
6. The RNeasy spin column was placed into a new 1.5 ml collection tube, and 50 µl of RNase-free water was added directly to the spin column membrane. The collection tube was centrifuged for 1 min at 8000G to elute the mRNA.

Extraction continued until a yield of >30 µg of RNA from each sample was reached. Samples were diluted using nuclease-free water to an RNA concentration of 5 ng/µL as determined using

a NanoDrop One (Cat. No. ND-ONE-W, ThermoFisher Scientific, Madison, WI). RNA samples were frozen at –80 °C before being transported to the Veterans Health Administration, Rocky Mountain Regional Veterans Affairs Medical Center (RMRVAMC) Core Equipment facility for analysis.

NanoString & Data Analysis

The NanoString RNA profiling technology uses reporter probes that bind to known sequences and can be read via optical scanner (*NCounter® Sprint Profiler*, n.d.). This RNAseq technology can be used to discover which mRNA transcripts a cell is producing and allows identification of any activated pathways. Jeremy T. Rahkola of the Rocky Mountain Regional VAMC Flow Core processed RNA for each of the 12 samples with the NanoString nCounter Sprint system (NanoString, Seattle, WA, USA) per vendor instructions with the nCounter Mouse Inflammation v2 Panel (Cat. No. XT-CSO-MIN2-12; NanoString Seattle, WA, USA). Sample RNA (25-100 ng) was mixed with the Reporter Codeset and Capture Probeset and then incubated at 65 °C for at least 16 hours to allow adequate hybridization. Hybridization buffer was used to bring the samples to 30 µL volume, which was then loaded into the cartridge and run on the nCounter Sprint profiler.

Data were RUV-III-normalized using nCounter (https://nanostring.com/) and RStudio (https://posit.co/) then analyzed via Rosalind (https://rosalind.bio/) with a HyperScale architecture developed by Rosalind, Inc. (San Diego, CA, USA). The limma R library (Ritchie et al., 2015) was used to calculate fold changes and *p*-values in Rosalind.

Results

Mycobacterium vs. BBS

When compared to the BBS (non-inflammatory) control, the novel strain of *Mycobacterium* induced a mild inflammatory reaction in the BV-2 cells. Complement component 3 (*C3*) is highly differentially expressed. Ranging between –0.91 in a BBS group sample and +0.91 in a *Mycobacterium* group sample (Fig. 2A). Out of the 248 genes in the screening panel, exposing the microglia to the novel strain of *Mycobacterium* significantly increased transcription of 14 genes, 5.6% of those measured, and significantly lowered expression levels for two genes (0.81%), *Il6ra* and *Arg1,* encoding interleukin 6 receptor, alpha and arginase 1 (a canonical marker of anti-inflammatory microglia), and *Il-6ra, which* encodes the receptor of pro-inflammatory *IL-6* (Cai et al., 2019, Feghali & Wright, 1997). 13 of the upregulated genes were pro-inflammatory genes and one, *Tnfaip3*, anti-inflammatory (Fig. 2B). Normalized data for each gene and sample is included after the discussion section in Fig. 2C.

Figure 2: Myco + BBS vs. BBS

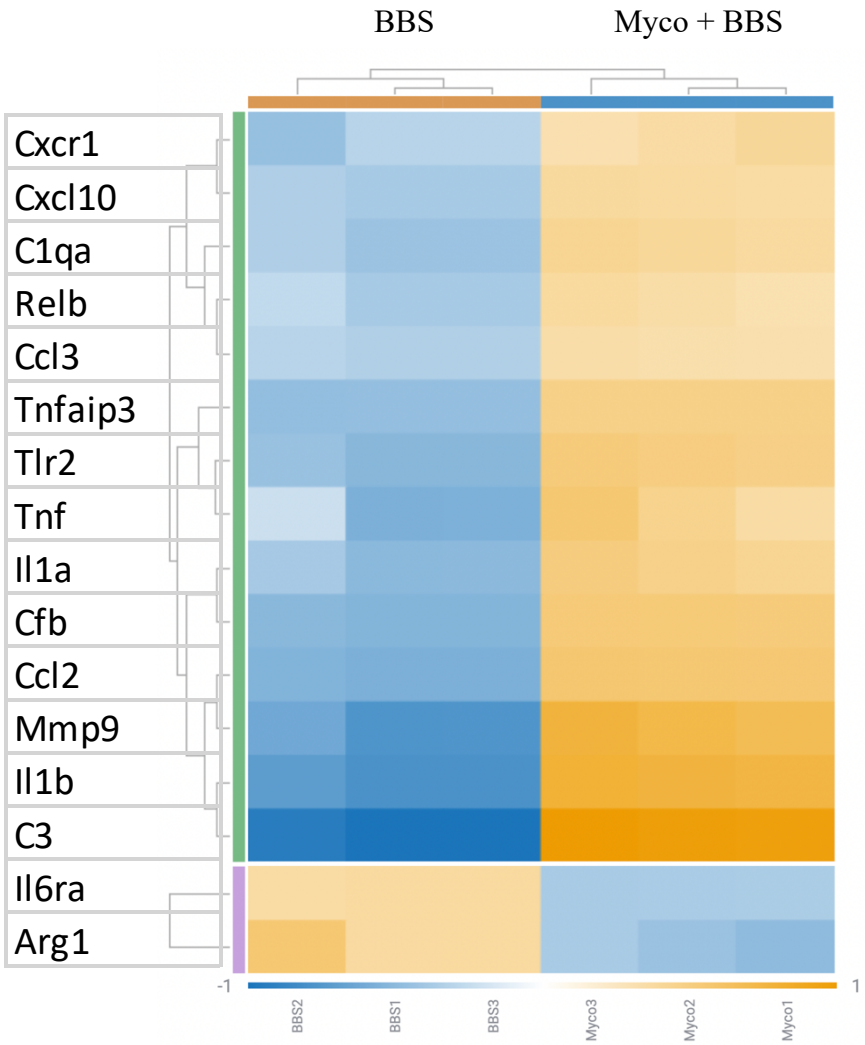

2A. The effect of the* M. smegmatis-*related strain. This heatmap displays *Z*-scores for genes with significantly differing levels of expression between the group treated with the *Mycobacterium* in a BBS vehicle and the group treated with just the BBS vehicle. Genes are marked along the Y-axis, with a green column representing genes whose expression levels increased due to environmental exposure to the *M. smegmatus*-related strain. The orange bar at the top of the heatmap represents BBS samples, with the blue bar representing *Mycobacterium* samples. The blue to orange gradient at the bottom of the heat map is a color legend relating the color of each cell to its fold change. This heatmap was generated using the Rosalind OnRamp NanoString gene expression analysis software (https://rosalind.bio/).

*Genes shown in heatmaps are revisualized in subsequent volcano plots.
**Names and properties of all tested genes are listed in a table at the end of this document.

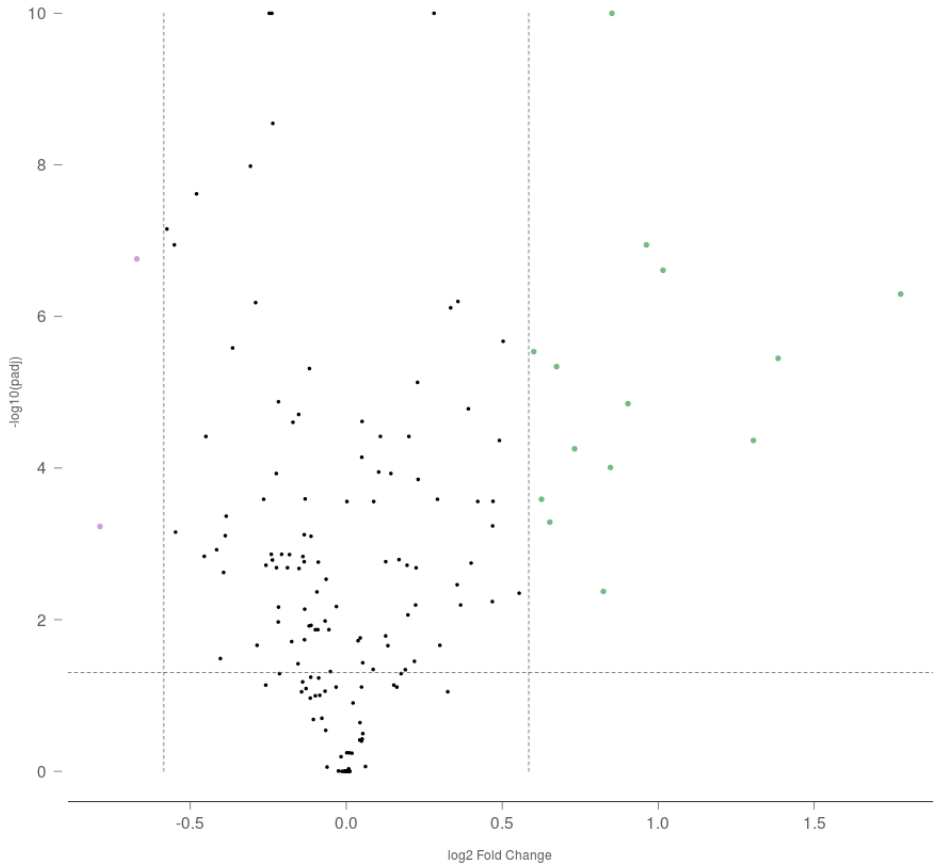

2B. Volcano plot visualization of differential expression levels between the Mycobacterium and borate-buffered saline (BBS) groups. The log2 ratio of the fold change is represented by the X-axis and the Y-axis shows the –log10 of adjusted *P*-values. Each point on the plot represents the difference in expression levels of a certain gene between the groups. Green points in the upper-right sextile of the plot represent genes whose expression levels increased in correlation with exposure to the *Mycobacterium*. Black points between the two vertical lines and points below the horizontal line represent genes with expression level differences that were not deemed statistically significant, and violet points represent genes with decreased expression. Genes with changes in concentration above 60% (log2 fold change ≥ 0.6) and an a –log10(p) of greater than 1.6 were flagged for interest. This volcano plot was generated using the Rosalind OnRamp NanoString gene expression analysis software (https://rosalind.bio/).

LPS + BBS vs. BBS

The addition of lipopolysaccharide (LPS), relative to the BBS vehicle, affected transcription levels more than addition of the *M. smegmatis*-related strain (Fig. 3). 50 of the 248 genes measured (20.2%) were transcribed at statistically different levels between treatment groups. 35 of them (14.1%) were upregulated by LPS, with the highest increases observed among the production of pro-inflammatory *Cfb*, *Ccl5*, and *Il-1β*. Fifteen genes (6.0%) were downregulated (Fig. 3, A&B). *Tnfaip3* is the only immunoregulatory transcript with statistically increased expression levels between groups. Inflammation-induced TNF production likely triggered this upregulation (Liu et al., 2022). Normalized data for each gene and sample is included after the discussion section in Fig. 3C.

Figure 3: LPS + BBS vs. BBS

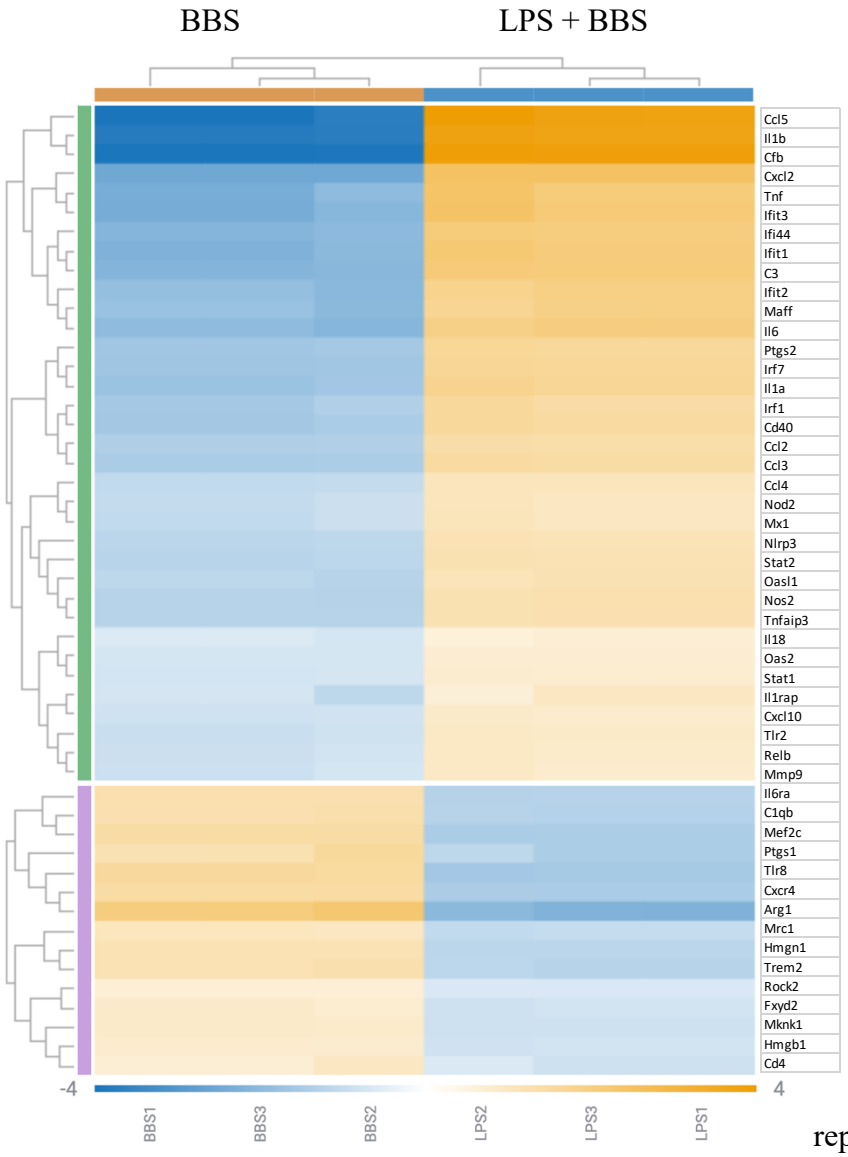

3A. Heatmap displaying Z-scores for genes with significantly differing levels of expression between the BBS and LPS + BBS groups. Genes are marked along the Y-axis, with a green column representing genes whose expression levels increased due to LPS exposure and a violet column denoting those whose expression levels decreased. The orange bar at the top of the heatmap represents BBS group samples and the blue bar represents LPS group samples. The blue to orange gradient at the bottom of the heat map is a color legend relating the color of each cell to its *Z*-score. This heat map was generated using the Rosalind OnRamp NanoString gene expression analysis software (https://rosalind.bio/).

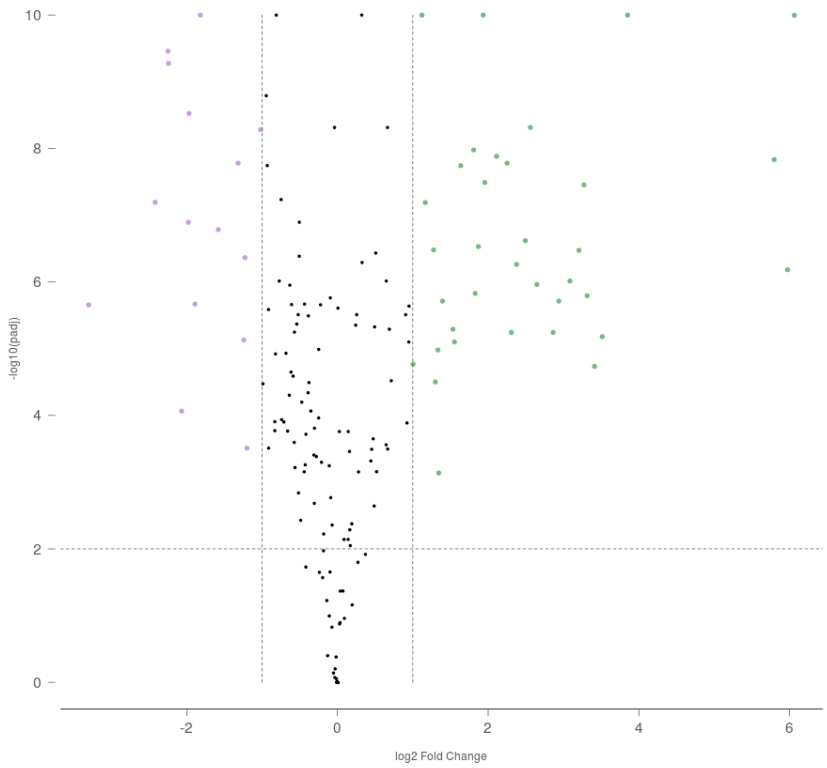

3B. Volcano plot visualization of differential expression levels between the LPS + BBS and BBS groups. The log2 ratio of the fold change is represented by the X-axis and the Y-axis shows the –log10 of adjusted *P*-values. Each point on the plot represents the difference in expression levels of a certain gene between the two groups. Green points in the upper-right sextile of the plot represent genes whose expression levels increased in correlation with LPS exposure, while violet points in the upper-left sextile of the plot represent those whose expression levels decreased. Black points between the two vertical lines and points below the horizontal line represent genes with expression level differences that were not deemed statistically significant. Genes with changes in concentration above 100% (log2 fold change ≥ 1) and an a –log10(*p*) of greater than 2 were flagged for interest. This volcano plot was generated using the Rosalind OnRamp NanoString gene expression analysis software (https://rosalind.bio/). Genes with

changes in concentration above 100% (log2 fold change ≥ 1) and an a –log10(p) of greater than 2 were flagged for interest.

LPS + BBS vs. Myco + BBS

The addition of LPS, relative to BBS vehicle, increased transcription levels of inflammation-related genes more than addition of the *M. smegmatis*-related strain (Fig. 2, 3). Forty-five of the 248 genes measured (18.1%) were transcribed at statistically different levels between treatment groups. Thirty-two of them (12.9%) were upregulated by LPS, with the highest increases observed among the production of pro-inflammatory *Cfb*, *Ccl5*, and *Il-1β*. Thirteen genes (6.0%) were downregulated (Fig. 4). *Tnfaip3* is the only immunoregulatory transcript with statistically increased expression levels in the LPS group. Inflammation-induced TNF production likely triggered this upregulation (Liu et al., 2022). Normalized data for each gene and sample is included after the discussion section in Fig. 4C.

Figure 4: LPS + BBS vs. Myco + BBS

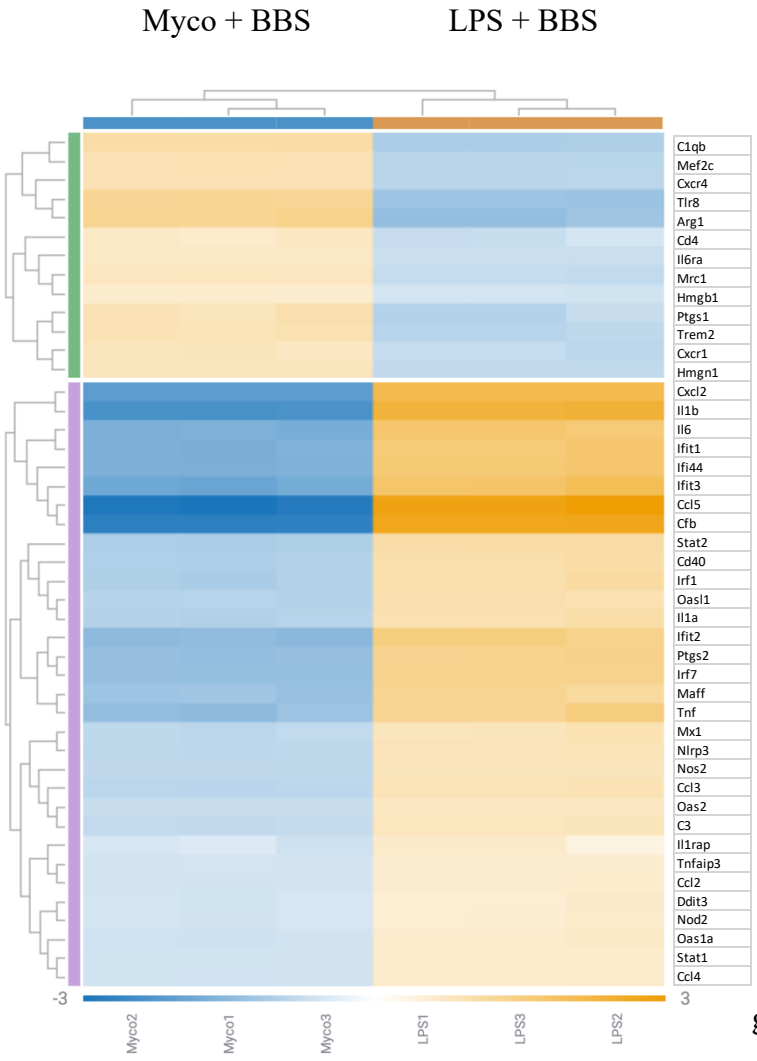

4A. Heatmap displaying Z-scores for genes with significantly differing levels of expression between the LPS + BBS and Myco + BBS groups. Genes are marked along the Y-axis, with a green column representing genes whose expression levels were lower in the LPS + BBS group than the Myco + BBS group. A violet column denotes those whose expression levels increased more in the LPS group. The orange bar at the top of the heatmap represents LPS + BBS group samples and the blue bar represents Myco + BBS group samples. The blue to orange gradient at the bottom of the heat map is a color legend relating the color of each cell to its *Z*-score. This heat map was generated using the Rosalind OnRamp NanoString gene expression analysis software (https://rosalind.bio/).

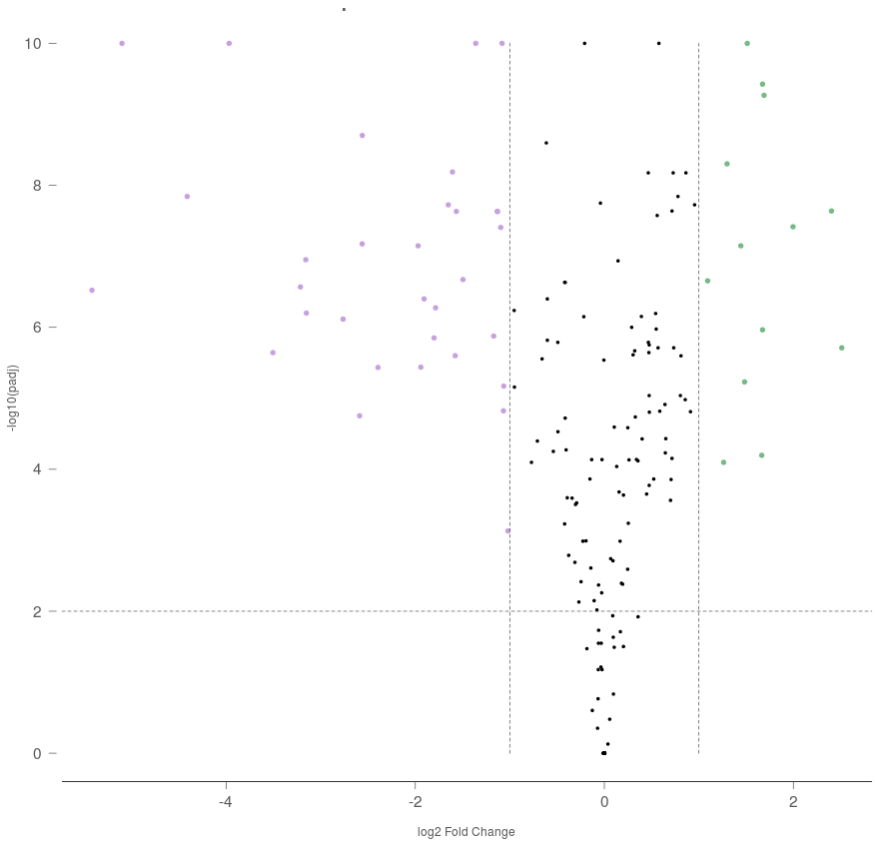

4B. Volcano plot visualization of differential expression levels between the LPS + BBS and Myco + BBS groups. The log2 ratio of the fold change is represented by the X-axis and the Y-axis shows the –log10 of adjusted P-values. Each point on the plot represents the difference in expression levels of a certain gene between the two groups. Green points in the upper-right sextile of the plot represent genes whose expression levels increased in correlation with LPS exposure, while violet points in the upper-left sextile of the plot represent those whose expression levels were comparatively decreased. Black points between the two vertical lines and points below the horizontal line represent genes with expression level differences that were not deemed statistically significant. Genes with changes in concentration above 100% (log2 fold change ≥ 1) and an a –log10(p) of greater than 2 were flagged for interest. This volcano plot was

generated using the Rosalind OnRamp NanoString gene expression analysis software (https://rosalind.bio/).

Myco + BBS vs Myco + LPS

Among *Mycobacterium* exposed cells, LPS exposure produced a stronger inflammatory response (Fig. 4, A&B). The genes most upregulated by the LPS + Myco group include *Ccl5, Cfb*, and *Cxcl2*. Increased transcription levels of these genes are associated with heightened inflammation (Queen et al., 2016). Mmong *Mycobacterium*-exposed cells, LPS decreased the expression of some genes. These include *Ptgs1*, the protein of which is involved in prostaglandin synthesis, and *C1qb*, in the complement pathway, both of which are associated with the pathogen-associated molecular pattern (PAMP) response (Queen et al., 2016). Although levels of mRNA for the anti-inflammatory gene *Tnfaip3* were higher among the LPS + Myco group, this is likely due to increased production of inflammatory TNF, which triggers *TNFAIP3* transcription (Liu et al., 2022). Exposure to LPS and mycobacteria appears to downregulate transcription of *Tlr8* and *CD4* when compared to *Mycobacterium* exposure alone. Upregulation of these genes is important for the propagation of the active immune response (Queen et al., 2016). Normalized data for each gene and sample is included after the discussion section in Fig. 5C.

Figure 5: Myco + BBS vs LPS + Myco

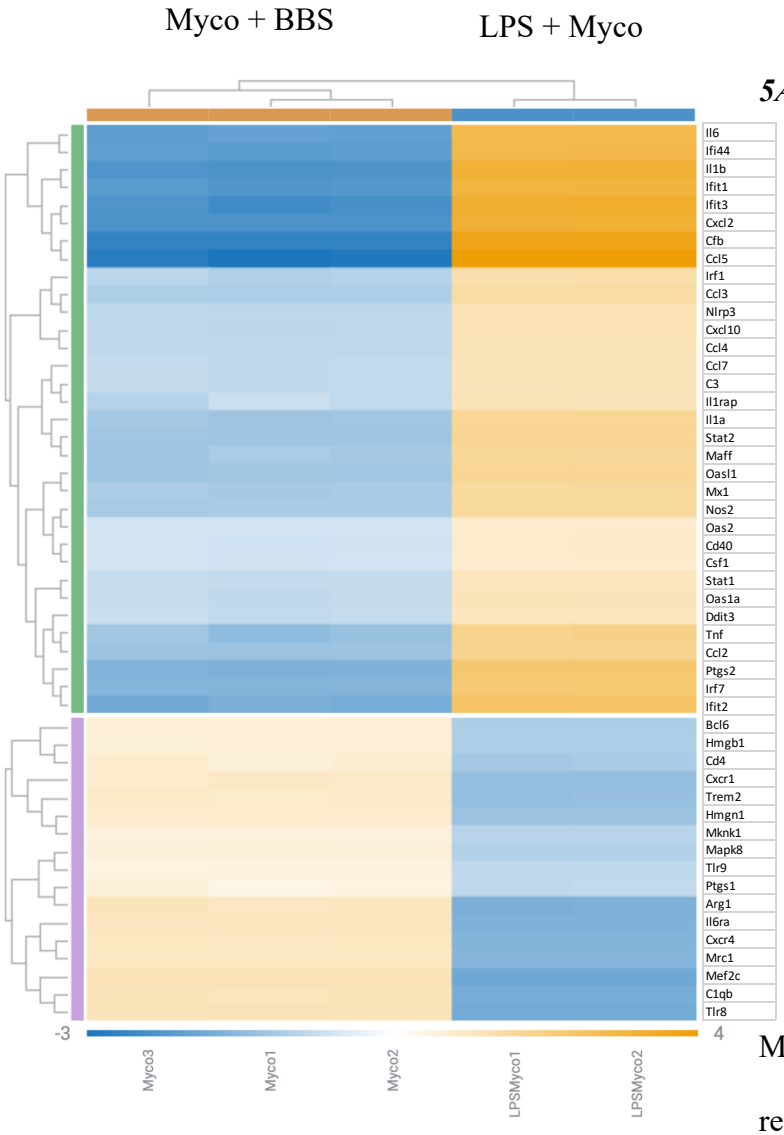

5A. Heatmap displaying Z-scores for genes with significantly differing levels of expression between the Myco group and the LPS + Myco group. Genes are marked along the Y-axis, with a green column representing genes whose expression levels increased due to LPS exposure in the presence of the *M. smegmatus*-related strain and a violet column denoting those whose expression levels decreased. The orange bar at the top of the heatmap represents Myco + BBS samples and the blue bar represents LPS + Myco samples. One replicate of LPS + *Myco* group was flagged for quality control by nCounter software and was excluded from this analysis. The blue to orange gradient at the bottom of the heat map is a color legend relating the color of each cell to its *Z*-score. This heatmap was generated using the Rosalind OnRamp NanoString gene expression analysis software (https://rosalind.bio/).

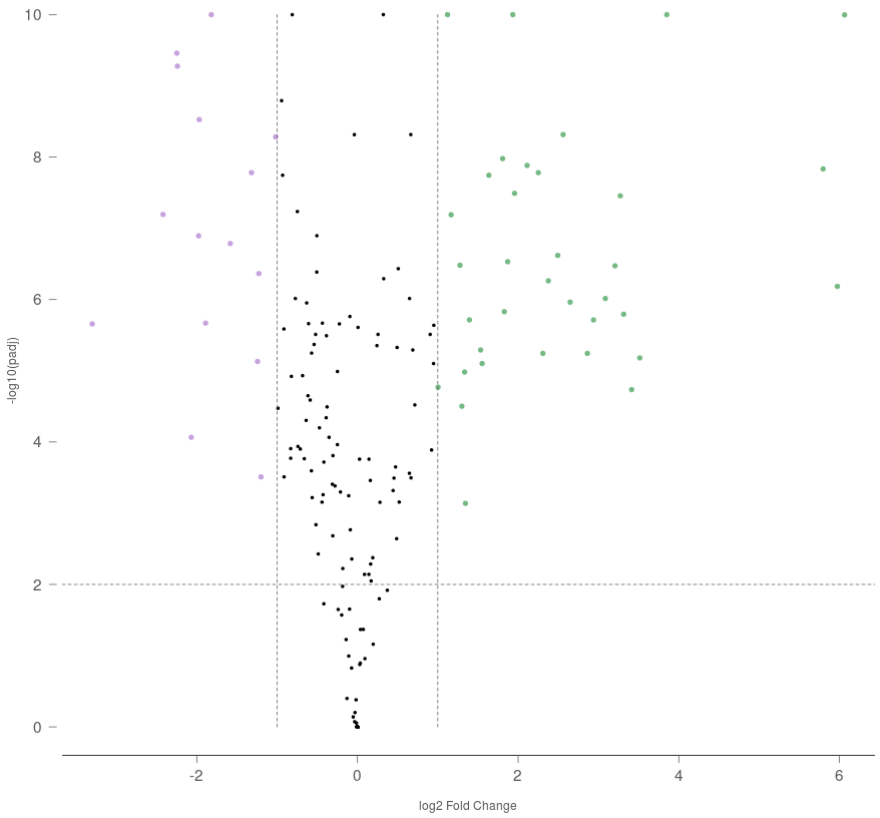

5B. Volcano plot visualization of differential expression levels between the Myco + BBS and LPS + Myco groups. The log2 ratio of the fold change is represented by the X-axis and the Y-axis shows the –log10 of adjusted *P*-values. Each point on the plot represents the difference in expression levels of a certain gene between the two groups. Green points in the upper-right sextile of the plot represent genes whose expression levels increased in correlation with LPS exposure in the presence of the *M. smegmatus*-related strain, while violet points in the upper-left sextile of the plot represent those whose expression levels decreased. Black points between the two vertical lines and points below the horizontal line represent genes with expression level differences that were not deemed statistically significant. Genes with changes in concentration above 100% (log2 fold change ≥ 1) and an a –log10(p) of greater than 2 were flagged for interest. This volcano plot was generated using the Rosalind OnRamp NanoString gene expression analysis software (https://rosalind.bio/).

LPS + BBS vs LPS + Myco

When compared to treatment with LPS + BBS, treatment with LPS and the novel *Mycobacterium* strain produced a stronger inflammatory response (Fig. 5, A&B). The genes most upregulated by the LPS + Myco group include *Ccl2* and *Ccl7*. Increased transcription levels of these genes at the onset of infection are associated with heightened monocyte and neutrophil activity (Bardina et al., 2015). Among the Mycobacteria-exposed cells, LPS increased transcription of 55 genes in the panel (22.1%) and decreased expression of 7 genes (2.8%): *Cxcr4, Mrc1, Myl2, Cd4, C1qb, Mef2c,* and *Trem2*. These genes also code for inflammation-causing molecules (Queen et al., 2016). Although levels of mRNA for the anti-inflammatory gene *Tnfaip3* were higher among the LPS + Myco group, this is likely due to increased production of inflammatory TNF, which triggers *Tnfaip3* transcription (Liu et al., 2022). Normalized data for each gene and sample is included after the discussion section in Fig. 6C.

Figure 6: LPS + BBS vs LPS + Myco

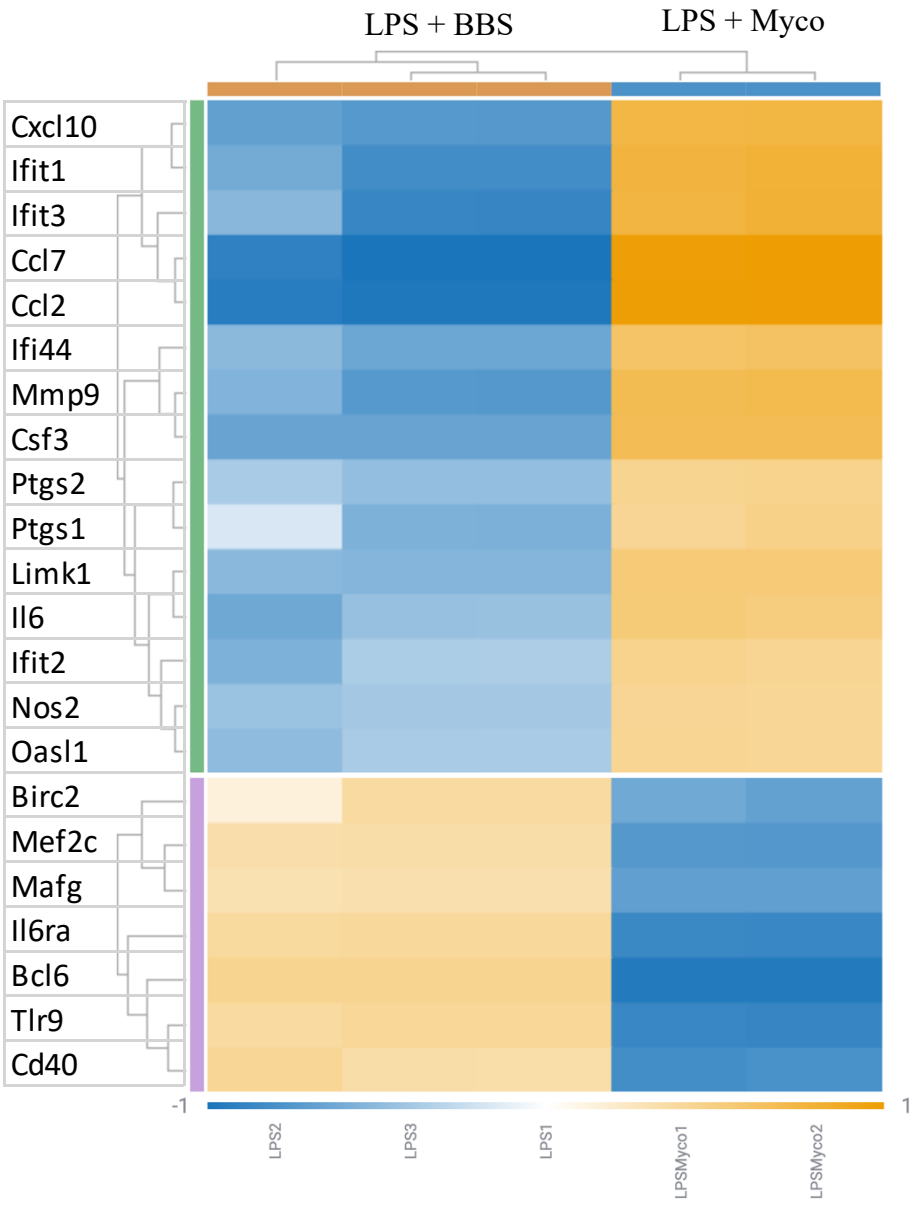

5A. Heatmap displaying Z-scores for genes with significantly differing levels of expression between the LPS + BBS group and the LPS + Myco group. Genes are marked along the Y-axis, with a green column representing genes whose expression levels increased due to LPS exposure in the presence of the *M. smegmatis*-related strain and a violet column denoting those whose expression levels decreased. The orange bar at the top of the heatmap represents LPS + BBS samples and the blue bar represents LPS + Myco samples. One replicate of LPS + *Myco* group was flagged for quality control by nCounter software and was excluded from this analysis. The blue to orange gradient at the bottom of the heat map is a color legend relating the

color of each cell to its *Z*-score. This heatmap was generated using the Rosalind OnRamp NanoString gene expression analysis software (https://rosalind.bio/).

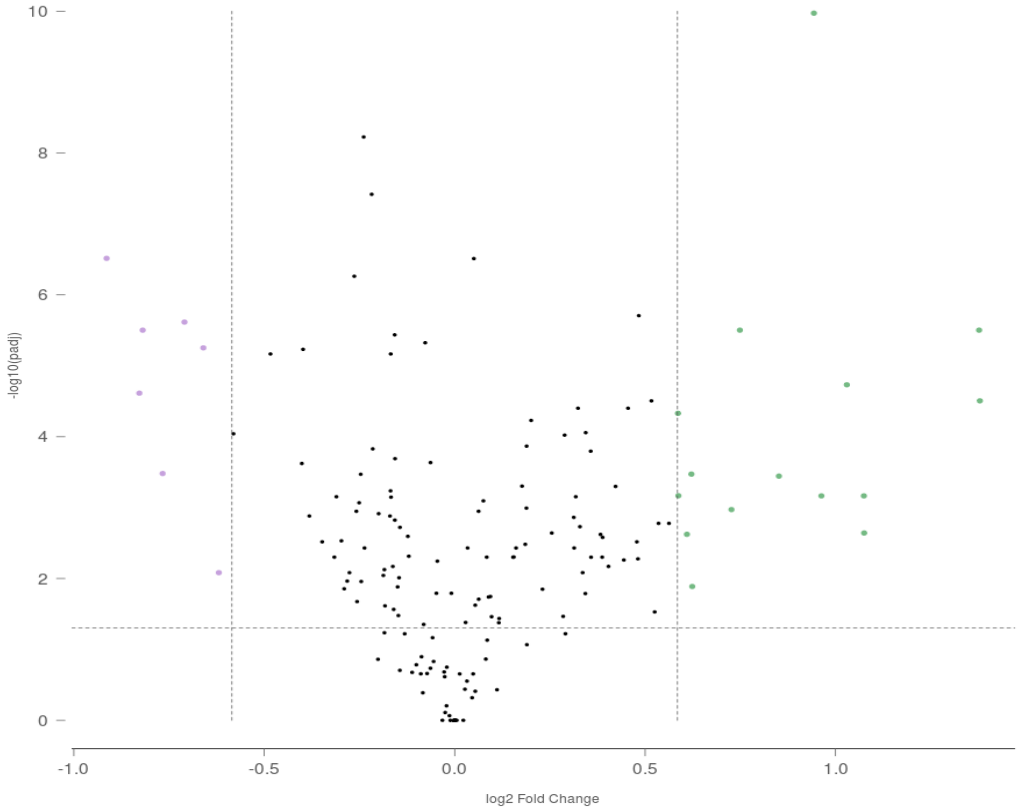

6B. Volcano plot visualization of differential expression levels between the LPS + BBS and LPS + Myco groups. The log2 ratio of the fold change is represented by the X-axis and the Y-axis shows the –log10 of adjusted *P*-values. Each point on the plot represents the difference in expression levels of a certain gene between the two groups. Green points in the upper-right sextile of the plot represent genes whose expression levels increased in correlation with LPS exposure in the presence of the *M. smegmatus*-related strain, while violet points in the upper-left sextile of the plot represent those whose expression was decreased among the Myco + BBS group. Black points between the two vertical lines and points below the horizontal line represent genes with expression level differences that were not deemed statistically significant. Genes with changes in concentration above 100% (log2 fold change ≥ 1) and an a –log10(p) of greater than 2

were flagged for interest. This volcano plot was generated using the Rosalind OnRamp NanoString gene expression analysis software (https://rosalind.bio/).

Other Genes of Interest (Compared across all groups)

Figure 7: *Il-10*

Interleukin 10 is an immunomodulatory cytokine known to decrease pro-inflammatory nuclear factor-κB (*Nf-κb*) activity (DRIESSLER et al., 2004). In tests with human THP-1 monocyte-derived macrophages, exposure to *M. vaccae* NCTC 11659 upregulated *Il-10* production (Holbrook et al., 2023). The novel strain did not appear to affect *Il-10* transcription levels between groups.

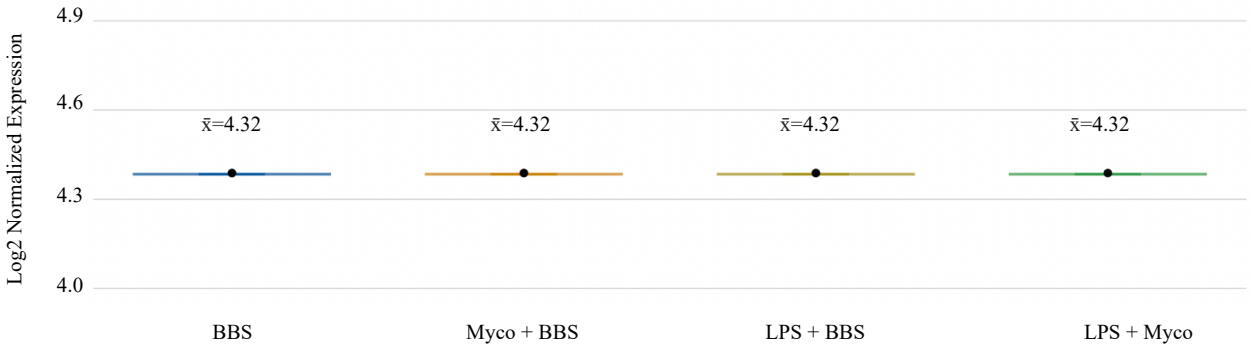

*Graphs generated using Rosalind.
**Plots show normalized levels of mRNA transcripts broken up by group (Y axis). The X axis represents the log2 of the normalized expression value. The mean for each group is denoted by x̄.

TNFAIP3, TNF & NF-κB

TNF-alpha induced protein 3 (*Tnfaip3*) is an *Nf-κb* inhibitor upregulated by tumor necrosis factor (TNF) (Kany et al., 2019). *Tnfaip3, Tnf*, and *Nf-κb* demonstrated proportional transcription level increases, as expected. Although the *TNFAIP3* gene codes for an immunoregulatory protein, in this case its previously identified increased expression indicates a functioning self-regulatory mechanism on the pro-inflammatory TNF and NF-κB protein products.

Figure 9: *TNFAIP3*

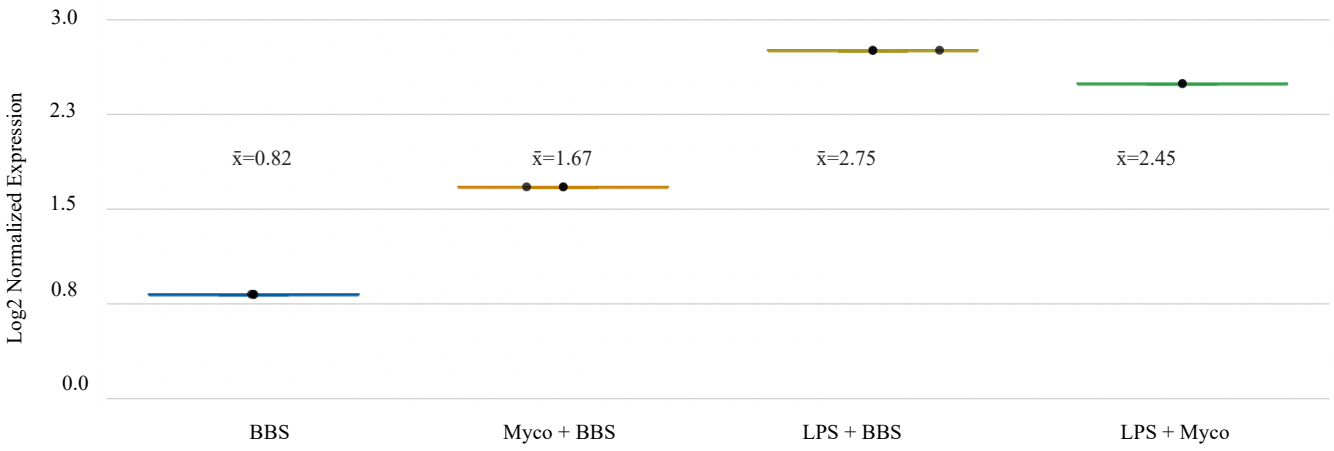

Figure 10: *TNF*

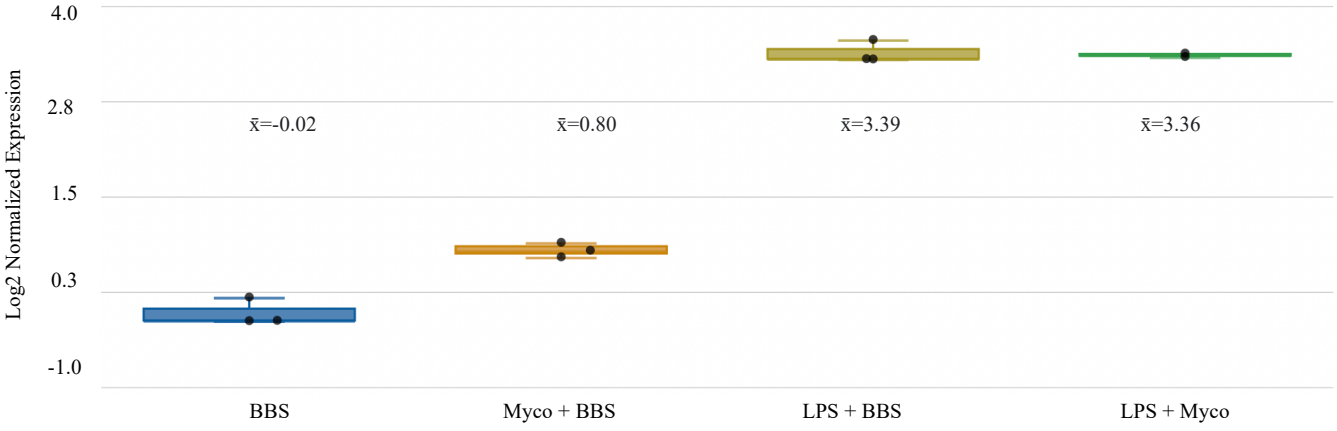

Figure 11: *NF-κB*

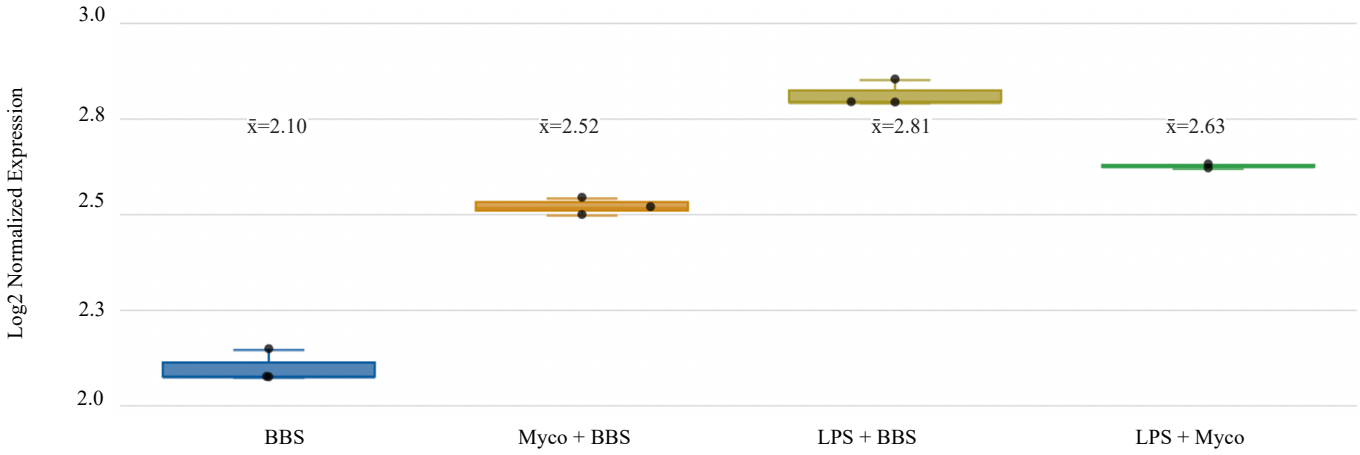

Figure 12: *CSF3*

The protein coded for by the colony stimulating factor 3 (*Csf3)* gene falls under the *Il-6* family and is pro-inflammatory. This cytokine is responsible for the activation of granulocytes and is commonly part of the "cytokine storm" experienced at the onset of illness (Boni et al., 2022). This gene appears to only be differentially expressed in the LPS + Myco group, which may indicate a reaction involving both the novel *Mycobacterium* and LPS.

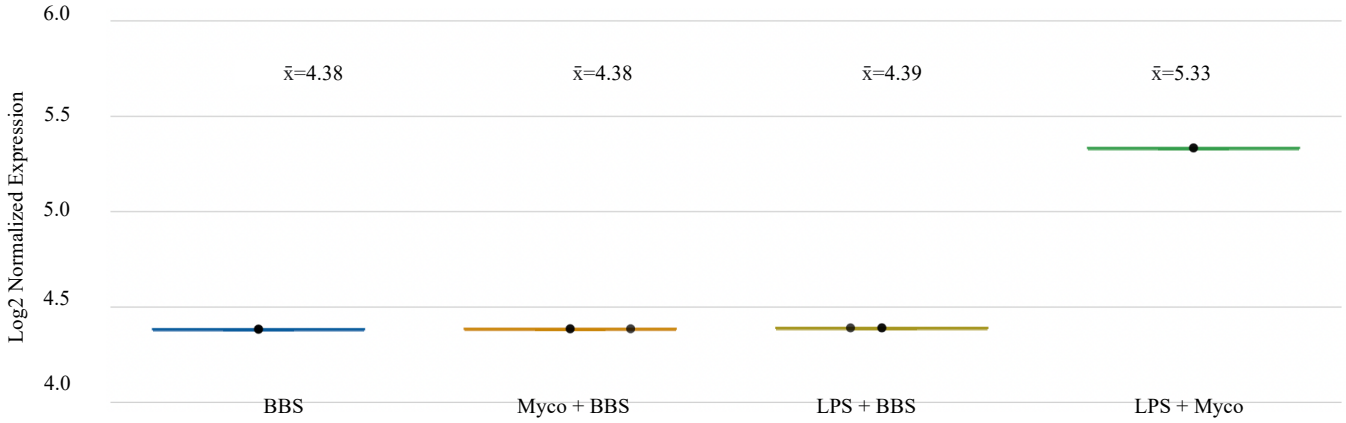

Figure 13: IL-6

Interleukin 6 is a pro-inflammatory cytokine that is key in initiating the innate immune response and microglial priming (Garner et al., 2018). These data are unexpected because the *Mycobacterium* did not appear to trigger *Il-6* production outside of the presence of LPS.

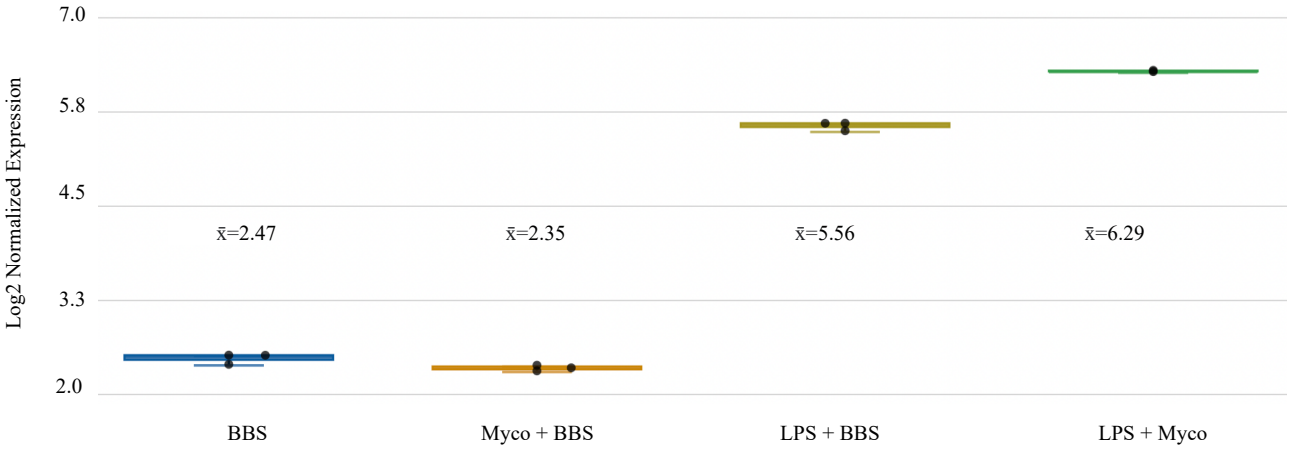

Figure 14: Spinal Cord Injury Response

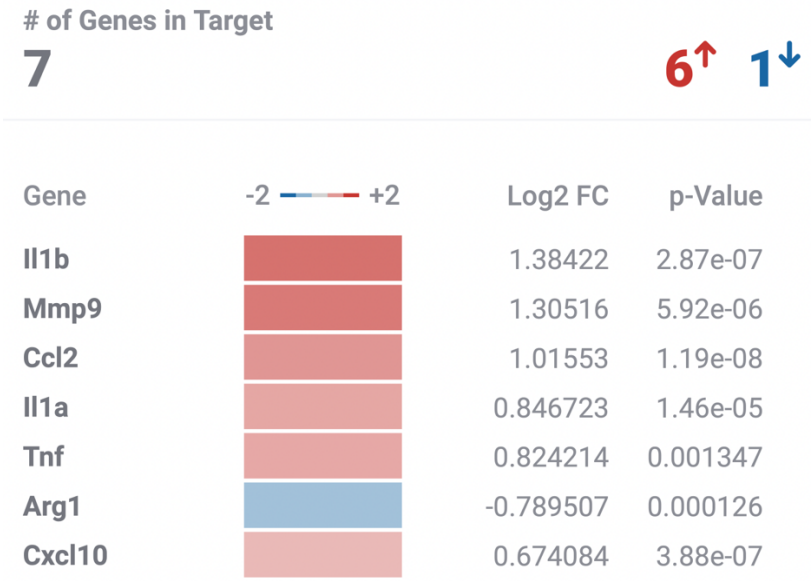

***14A. Spinal cord injury-associated genes upregulated by the novel* Mycobacterium.** Pathway analysis performed using Rosalind (https://rosalind.bio/) and data from WikiPathways (Martens

et al., 2021) revealed activation of the spinal cord injury response pathway. These inflammation-linked genes were upregulated in the Myco + BBS group when compared to the BBS group, indicating that the BV-2 cells recognized the novel *Mycobacterium* as pathogenic. *Arg1*, a key marker of anti-inflammatory microglia, is the only gene in the screen whose transcription levels decreased (Cai et al., 2019). Includes the log2 of the fold change (increase or decrease in expression) and adjusted *p*-values. Full pathway analysis in Fig. 14B, included after the discussion section on page 43.

Discussion

C3 is a key component of the innate immune system's classical pathway that opsonizes potential pathogens and communicates inflammatory signals between nearby cells (Geisbrecht et al., 2022). Microglia are the main producers of C3 in the dentate gyrus of the hippocampus (Bourel et al., 2021). Experimental autoimmune encephalomyelitis (EAE), a demyelinating disease, is often used as a model for multiple sclerosis (MS) in murine trials investigating neurodegeneration. In EAE mice, C3 and other inflammatory cytokines are produced by overactive microglia and cause memory impairment, as well as early dendritic loss and microglia-mediated phagocytosis of synapses in the dentate gyrus. Inhibiting the microglial production of C3 prevented or eased these symptoms, regardless of other microglial activation markers (Bourel et al., 2021). Similar damage to the substantia nigra is thought to influence the development of Parkinson's disease, and deteriorating basal ganglia often can contribute to palsies and vision impairment (Mercuri et al., 1997). As the novel strain of *Mycobacterium* consistently increases transcription of *C3*, microgliosis and damage to neural tissue may overshadow any of its immunoregulatory characteristics if in direct contact with the CNS.

Although the novel strain of *Mycobacterium* did not trigger inflammatory *Il-6* production, it is unlikely to alleviate any inflammation related to mental health conditions. The strain's prominent upregulation of other pro-inflammatory genes, including *C3, IL-1α,* and IL-*1β,* likely eliminates any possibility of using it as a direct-contact anti-inflammatory agent on microglia. The BV-2 cells also recognized the bacteria as pathogenic and activated the spinal cord injury response. *Cxcr1* was the only gene downregulated more by the *Mycobacterium* in comparison to LPS than by BBS when compared to LPS (Figs. 3&4). Three genes, *Rock2*, *FxyD2*, and *MKNK1* were upregulated by the *Mycobacteria* and downregulated by BBS. Among these genes, the *Mycobacteria* was more pro-inflammatory than LPS. As microglial cells generally remain isolated from contact with bacteria, their responses may not be generalizable across other immune cell lineages. The BV-2 cells also recognized the bacteria as pathogenic and activated the spinal cord injury response. These mycobacteria are clearly inflammatory in neural tissue. Leukocytes that circulate through peripheral tissue, such as macrophages, and those that express *CD4*, such as helper T and Treg lymphocytes, would be ideal subjects for future studies on immune reactions to this strain of bacterium. The nCounter Mouse Inflammation v2 Panel (Cat. No. XT-CSO-MIN2-12; NanoString Seattle, WA) did not measure *MHCII* transcript concentrations. Especially in conjunction with B- and T- lymphocytes, any effect on antigen presenting proteins could generate new immunological responses and should be investigated (Frank et al., 2006).

Genomic analysis and peptide staining would lead to a better understanding of the novel strain's surface protein composition and reveal the mechanisms behind its interactions with somatic cells. Although the *Mycobacterium* induced a pro-inflammatory response, its apparent lack of

effect on IL6, and possibly CSF3, transcription levels make it an appealing target for further immunological research regarding the transcription of these cytokines. When analyzed in conjunction with more likely “old friend” species, these data could accelerate the development of new anti-inflammatory therapeutics or aid in the engineering of recombinant strains with select immunomodulatory properties.

Additional Figures:

Normalized expression data tables:

Gene Name	BBS2	BBS1	BBS3	Myco3	Myco2	Myco1	Cluster
Cxcr1	-0.4143538	-0.2813638	-0.2830938	0.28437917	0.32862517	0.36580717	1
Cxcl10	-0.3125017	-0.3495517	-0.3490717	0.34870833	0.33638833	0.32602833	1
C1qa	-0.312315	-0.393265	-0.392205	0.391425	0.364495	0.341865	1
Relb	-0.2435717	-0.3483717	-0.3470117	0.34599833	0.31112833	0.28182833	1
Ccl3	-0.28129	-0.31034	-0.30996	0.30968	0.30002	0.29189	1
Tnfaip3	-0.4273267	-0.4249797	-0.4250107	0.42503233	0.42581233	0.42647233	1
Tlr2	-0.4070315	-0.4741345	-0.4732595	0.4726085	0.4502885	0.4315285	1
Tnf	-0.2070085	-0.5166745	-0.5126385	0.5096455	0.4066235	0.3200525	1
Il1a	-0.3516108	-0.4599422	-0.4585305	0.45748318	0.42144318	0.39115718	1
Cfb	-0.4685572	-0.4873472	-0.4871022	0.48691883	0.48066883	0.47541883	1
Ccl2	-0.4913017	-0.5161617	-0.5158317	0.51558833	0.50732833	0.50037833	1
Mmp9	-0.563045	-0.698235	-0.696465	0.695165	0.650185	0.612395	1
Il1b	-0.6451155	-0.7160655	-0.7151455	0.7144585	0.6908525	0.6710155	1
C3	-0.8539783	-0.9063783	-0.9056983	0.90519167	0.88776167	0.87310167	1
Il6ra	0.32590167	0.34076167	0.34057167	-0.3404283	-0.3354783	-0.3313283	2
Arg1	0.50567667	0.33819667	0.34038667	-0.3420033	-0.3977133	-0.4445433	2

Figure 2C. Normalized expression levels of significantly differentially expressed genes between the BBS and Myco + BBS groups. Treatment groups are labeled in the top row, with a number 1-3 denoting the sample. Each gene symbol is further defined in the gene table. Cluster 1 genes experienced increased transcription in the presence of the *Mycobacterium*, while cluster 2 genes were decreased.

Gene Name	BBS1 (BBS)	BBS3 (BBS)	BBS2 (BBS)	LPS2 (LPS)	LPS3 (LPS)	LPS1 (LPS)	Cluster
Ccl5	-3.058795	-3.056035	-2.846365	3.102835	2.930515	2.927845	1
Il1b	-2.9222417	-2.9213217	-2.8512917	2.93694833	2.87939833	2.87850833	1
Cfb	-3.0383755	-3.0381305	-3.0195855	3.0422705	3.0270305	3.0267905	1
Cxcl2	-1.923193	-1.923279	-1.929833	1.921815	1.927205	1.927285	1
Tnf	-1.8109642	-1.8069282	-1.5012982	1.87514683	1.62396683	1.62007683	1
Ifit3	-1.8396133	-1.8364233	-1.5953033	1.89024567	1.69208267	1.68901167	1
Ifi44	-1.63514	-1.63391	-1.54107	1.65464	1.57833	1.57715	1
Ifit1	-1.707755	-1.705785	-1.557005	1.738995	1.616725	1.614825	1
C3	-1.6537417	-1.6530617	-1.6013417	1.66460833	1.62209833	1.62143833	1
Ifit2	-1.4220315	-1.4238705	-1.5631245	1.3927855	1.5072355	1.5090055	1
Maff	-1.3665067	-1.3690067	-1.5582267	1.32676333	1.48228333	1.48469333	1
Il6	-1.5015183	-1.5031083	-1.6236983	1.47619167	1.57530167	1.57683167	1
Ptgs2	-1.2690834	-1.2682234	-1.2028334	1.28281563	1.22907853	1.22824593	1
Irf7	-1.2877152	-1.2874192	-1.2650182	1.29242083	1.27401083	1.27372083	1
Il1a	-1.3604082	-1.3589965	-1.2520768	1.38286718	1.29498718	1.29362718	1
Irf1	-1.2061017	-1.2040817	-1.0515317	1.23813833	1.11275833	1.11081833	1
Cd40	-1.2155507	-1.2145007	-1.1349707	1.23225433	1.16689033	1.16587733	1
Ccl2	-1.0642717	-1.0639417	-1.0394117	1.06941833	1.04925833	1.04894833	1
Ccl3	-1.13567	-1.13529	-1.10662	1.14169	1.11813	1.11776	1
Ccl4	-0.8254382	-0.8251512	-0.8034292	0.83000283	0.81214283	0.81187283	1
Nod2	-0.799861	-0.798571	-0.701151	0.820314	0.740255	0.739014	1
Mx1	-0.8145955	-0.8131145	-0.7009205	0.8381535	0.7459535	0.7445235	1
Nlrp3	-0.9104287	-0.9101697	-0.8904987	0.91456233	0.89839233	0.89814233	1
Stat2	-0.953008	-0.952328	-0.900538	0.963888	0.921323	0.920663	1
Oasl1	-0.886643	-0.887701	-0.967829	0.869811	0.935671	0.936691	1
Nos2	-0.9677433	-0.9681333	-0.9981733	0.96142667	0.98611667	0.98650667	1
Tnfaip3	-0.965798	-0.965829	-0.968145	0.965314	0.967214	0.967244	1
Il18	-0.4717766	-0.4729386	-0.5609466	0.45329383	0.52562343	0.52674443	1
Oas2	-0.5609175	-0.5609125	-0.5605535	0.5609925	0.5606975	0.5606935	1
Stat1	-0.5907147	-0.5904247	-0.5685847	0.59529733	0.57735233	0.57707433	1
Il1rap	-0.5641617	-0.5683317	-0.8839017	0.49789833	0.75723833	0.76125833	1
Cxcl10	-0.6507217	-0.6502417	-0.6136717	0.65839833	0.62834833	0.62788833	1
Tlr2	-0.7193928	-0.7185178	-0.6522898	0.73330017	0.67887017	0.67803017	1
Relb	-0.702455	-0.701095	-0.597655	0.724185	0.639165	0.637855	1
Mmp9	-0.6954283	-0.6936583	-0.5602383	0.72344167	0.61379167	0.61209167	1
Il6ra	0.989885	0.989695	0.975025	-0.992935	-0.980935	-0.980735	2
C1qb	0.97389	0.974472	1.018552	-0.964638	-1.000858	-1.001418	2
Mef2c	1.12410683	1.12396583	1.11329583	-1.1263462	-1.1175762	-1.1174462	2
Ptgs1	0.94072567	0.94433967	1.21808367	-0.8832363	-1.1082163	-1.1116963	2
Tlr8	1.22522333	1.22463333	1.17982333	-1.2346367	-1.1978067	-1.1972367	2
Cxcr4	1.1212625	1.1213875	1.1308415	-1.1192805	-1.1270405	-1.1271705	2
Arg1	1.59418	1.59637	1.76166	-1.55947	-1.69532	-1.69742	2
Mrc1	0.804555	0.804055	0.766365	-0.812465	-0.781495	-0.781015	2
Hmgn1	0.9085745	0.9086145	0.9116465	-0.9079385	-0.9104285	-0.9104685	2
Trem2	0.91372017	0.91494417	1.00763117	-0.8942538	-0.9704308	-0.9716108	2
Rock2	0.51264483	0.51252283	0.50323483	-0.5145942	-0.5069642	-0.5068442	2
Fxyd2	0.65201867	0.65084867	0.56292867	-0.6704793	-0.5982183	-0.5970983	2
Mknk1	0.665375	0.665155	0.648425	-0.668885	-0.655145	-0.654925	2
Hmgb1	0.62697333	0.62646333	0.58803333	-0.6350467	-0.6034567	-0.6029667	2
Cd4	0.523953	0.526898	0.74995	-0.47711	-0.660425	-0.663266	2

Figure 3C. Normalized expression levels of significantly differentially expressed genes between the BBS and LPS + BBS groups. Treatment groups are labeled in the top row, with a number 1-3 denoting the sample. Each gene symbol is further defined in the gene table. Cluster 1 genes experienced increased transcription in the presence of the LPS, while cluster 2 genes were decreased.

Gene Name	Myco2 (Myc	Myco1 (Myc	Myco3 (Myc	LPS1 (LPS)	LPS3 (LPS)	LPS2 (LPS)	Cluster
C1qb	0.99718533	0.98469933	1.01204333	-1.0104227	-1.0098627	-0.9736427	1
Mef2c	0.84509033	0.84811233	0.84149333	-0.8418887	-0.8420187	-0.8507887	1
Cxcr4	0.83684083	0.83416383	0.84002783	-0.8396842	-0.8395542	-0.8317942	1
Tlr8	1.20232833	1.21502833	1.18722833	-1.1888717	-1.1894417	-1.2262717	1
Arg1	1.25302333	1.20619333	1.30873333	-1.3026667	-1.3005667	-1.1647167	1
Cd4	0.62703033	0.56385033	0.70221733	-0.6940317	-0.6911907	-0.5078757	1
Il6ra	0.64939	0.65354	0.64444	-0.64499	-0.64519	-0.65719	1
Mrc1	0.72284167	0.73351167	0.71013167	-0.7115183	-0.7119983	-0.7429683	1
Hmgb1	0.547075	0.557955	0.534115	-0.535525	-0.536015	-0.567605	1
Ptgs1	0.82766667	0.75012667	0.91994067	-0.9098913	-0.9064113	-0.6814313	1
Trem2	0.835128	0.808873	0.866372	-0.86297	-0.86179	-0.785613	1
Cxcr1	0.7443135	0.7814955	0.7000675	-0.7048855	-0.7065555	-0.8144355	1
Hmgn1	0.755997	0.755138	0.757019	-0.756908	-0.756868	-0.754378	1
Cxcl2	-1.9842822	-1.9824262	-1.9864912	1.98624983	1.98616983	1.98077983	2
Il1b	-2.2074325	-2.2272695	-2.1838265	2.1863995	2.1872895	2.2448395	2
Il6	-1.6051233	-1.5709733	-1.6457733	1.64134667	1.63981667	1.54070667	2
Ifit1	-1.57846	-1.62061	-1.52831	1.53377	1.53567	1.65794	2
Ifi44	-1.5805667	-1.6068567	-1.5492667	1.55267333	1.55385333	1.63016333	2
Ifit3	-1.757075	-1.825375	-1.675805	1.68465	1.687721	1.885884	2
Ccl5	-2.7136467	-2.7730367	-2.6429667	2.65066333	2.65333333	2.82565333	2
Cfb	-2.5513617	-2.5566117	-2.5451117	2.54578833	2.54602833	2.56126833	2
Stat2	-0.985828	-1.000498	-0.968378	0.970273	0.970933	1.013498	2
Cd40	-0.9545707	-0.9770907	-0.9277607	0.93067733	0.93169033	0.99705433	2
Irf1	-0.9733483	-1.0165583	-0.9219183	0.92752167	0.92946167	1.05484167	2
Oasl1	-0.8910018	-0.8683058	-0.9180118	0.91507317	0.91405317	0.84819317	2
Il1a	-0.902384	-0.93267	-0.866344	0.870266	0.871626	0.959506	2
Ifit2	-1.3792113	-1.3397673	-1.4261503	1.42103967	1.41926967	1.30481967	2
Ptgs2	-1.281865	-1.300385	-1.259825	1.26222427	1.26305687	1.31679397	2
Irf7	-1.2806565	-1.2870015	-1.2731055	1.2739245	1.2742145	1.2926245	2
Maff	-1.1937633	-1.1401633	-1.2575533	1.25060667	1.24819667	1.09267667	2
Tnf	-1.2997733	-1.3863443	-1.1967513	1.20796967	1.21185967	1.46303967	2
Mx1	-0.7907063	-0.8224853	-0.7528883	0.75700667	0.75843667	0.85063667	2
Nlrp3	-0.8036565	-0.8092282	-0.797026	0.7977469	0.7979969	0.8141669	2
Nos2	-0.781835	-0.773325	-0.791965	0.790865	0.790475	0.765785	2
Ccl3	-0.82584	-0.83397	-0.81618	0.81723	0.8176	0.84116	2
Oas2	-0.6800867	-0.6801887	-0.6799657	0.67997933	0.67998333	0.68027833	2
C3	-0.7482867	-0.7629467	-0.7308567	0.73275333	0.73341333	0.77592333	2
Il1rap	-0.5038317	-0.4144417	-0.6102017	0.59861833	0.59459833	0.33525833	2
Tnfaip3	-0.5407783	-0.5401183	-0.5415583	0.54147167	0.54144167	0.53954167	2
Ccl2	-0.5485467	-0.5554967	-0.5402867	0.54118333	0.54149333	0.56165333	2
Ddit3	-0.5355463	-0.5695122	-0.4951262	0.49952485	0.50105485	0.59960485	2
Nod2	-0.5336427	-0.5612327	-0.5008127	0.50438233	0.50562333	0.58568233	2
Oas1a	-0.586536	-0.60587	-0.563527	0.566031	0.566901	0.623001	2
Stat1	-0.5647097	-0.5708897	-0.5573497	0.55814933	0.55842733	0.57637233	2
Ccl4	-0.5669533	-0.5731033	-0.5596233	0.56042667	0.56069667	0.57855667	2

Figure 4C. Normalized expression levels of significantly differentially expressed genes between the LPS + BBS and Myco + BBS groups. Treatment groups are labeled in the top row, with a number 1-3 denoting the replicate. Each gene symbol is further defined in the gene table. Cluster 1 genes experienced increased transcription in the presence of the *Mycobacterium* and LPS, while cluster 2 genes were more highly expressed in the Myco + BBS group.

Gene Name	Myco3 (Myc	Myco1 (Myc	Myco2 (Myc	LPSMyco1 (L	LPSMyco2 (L	Cluster
Il6	-1.615016	-1.540216	-1.574366	2.373534	2.356064	1
Ifi44	-1.574012	-1.631602	-1.605312	2.398738	2.412188	1
Il1b	-1.7419966	-1.7854396	-1.7656026	2.6414494	2.6515894	1
Ifit1	-1.642916	-1.735216	-1.693066	2.524824	2.546374	1
Ifit3	-1.75527	-1.90484	-1.83654	2.73086	2.76579	1
Cxcl2	-1.7829492	-1.7788842	-1.7807402	2.6717618	2.6708118	1
Cfb	-2.040142	-2.051642	-2.046392	3.067748	3.070428	1
Ccl5	-2.145382	-2.275452	-2.216062	3.303268	3.333628	1
Irf1	-0.683122	-0.777762	-0.734552	1.086668	1.108768	1
Ccl3	-0.793996	-0.811786	-0.803656	1.202644	1.206794	1
Nlrp3	-0.6478446	-0.6600468	-0.6544751	0.97975828	0.98260828	1
Cxcl10	-0.64114	-0.66382	-0.65346	0.97656	0.98186	1
Ccl4	-0.628388	-0.641868	-0.635718	0.951412	0.954562	1
Ccl7	-0.5894348	-0.6266848	-0.6096748	0.9085482	0.9172462	1
C3	-0.594286	-0.626376	-0.611716	0.912444	0.919934	1
Il1rap	-0.718352	-0.522592	-0.611982	0.949318	0.903608	1
Il1a	-0.9003648	-0.9666908	-0.9364048	1.3939852	1.4094752	1
Stat2	-0.940386	-0.972506	-0.957836	1.431614	1.439114	1
Maff	-0.960574	-0.843184	-0.896784	1.363976	1.336566	1
Oasl1	-0.9744852	-0.9247792	-0.9474752	1.4291698	1.4175698	1
Mx1	-0.820209	-0.889806	-0.858027	1.275896	1.292146	1
Nos2	-0.869996	-0.851356	-0.859866	1.292784	1.288434	1
Oas2	-0.448378	-0.448601	-0.448499	0.672713	0.672765	1
Cd40	-0.4303732	-0.4797032	-0.4571832	0.6778698	0.6893898	1
Csf1	-0.431792	-0.459032	-0.446592	0.665528	0.671888	1
Stat1	-0.5821184	-0.5956584	-0.5894784	0.8820466	0.8852086	1
Oas1a	-0.5780168	-0.6203598	-0.6010258	0.8947612	0.9046412	1
Ddit3	-0.5433692	-0.6177552	-0.5837893	0.86377182	0.88114182	1
Tnf	-0.9250174	-1.1146104	-1.0280394	1.5117036	1.5559636	1
Ccl2	-0.981448	-0.996658	-0.989708	1.482132	1.485682	1
Ptgs2	-1.252288	-1.292848	-1.274328	1.904997	1.914467	1
Irf7	-1.2236866	-1.2375826	-1.2312376	1.8446334	1.8478734	1
Ifit2	-1.3937344	-1.3073514	-1.3467954	2.0340256	2.0138556	1
Bcl6	0.55352	0.54982	0.55152	-0.82788	-0.82698	2
Hmgb1	0.5251618	0.5490018	0.5381218	-0.8033592	-0.8089262	2
Cd4	0.6565624	0.5181954	0.5813754	-0.8942166	-0.8619166	2
Cxcr1	0.6677244	0.7491524	0.7119704	-1.0549186	-1.0739286	2
Trem2	0.7338626	0.6763636	0.7026186	-1.0631374	-1.0497074	2
Hmgn1	0.6688234	0.6669424	0.6678014	-1.0020036	-1.0015636	2
Mknk1	0.462688	0.473068	0.468328	-0.700832	-0.703252	2
Mapk8	0.509106	0.501476	0.504966	-0.758664	-0.756884	2
Tlr9	0.420182	0.440312	0.431122	-0.643458	-0.648158	2
Ptgs1	0.5039472	0.3341332	0.4116732	-0.6447008	-0.6050528	2
Arg1	0.920298	0.817758	0.864588	-1.313292	-1.289352	2
Il6ra	0.842302	0.851402	0.847252	-1.269428	-1.271528	2
Cxcr4	0.831873	0.826009	0.828686	-1.243969	-1.242599	2
Mrc1	0.798014	0.821394	0.810724	-1.212336	-1.217796	2
Mef2c	0.9563396	0.9629586	0.9599366	-1.4388424	-1.4403924	2
C1qb	0.9157328	0.8883888	0.9008748	-1.3556932	-1.3493032	2
Tlr8	0.911274	0.939074	0.926374	-1.385116	-1.391606	2

Figure 5C. Normalized expression levels of significantly differentially expressed genes between the Myco + BBS and Myco + LPS groups. Treatment groups are labeled in the top row, with a number 1-3 denoting the replicate. Each gene symbol is further defined in the gene table. Cluster 1 genes experienced increased transcription in the presence of the *Mycobacterium* and LPS, while cluster 2 genes were more highly expressed in the Myco + BBS group.

Gene Name	LPS2 (LPS)	LPS3 (LPS)	LPS1 (LPS)	LPSMyco1 (L	LPSMyco2 (L	Cluster
Cxcl10	-0.391684	-0.421734	-0.422194	0.615156	0.620456	1
Ifit1	-0.347618	-0.469888	-0.471788	0.633872	0.655422	1
Ifit3	-0.296883	-0.495046	-0.498117	0.627558	0.662488	1
Ccl7	-0.5184318	-0.5677888	-0.5685538	0.8230382	0.8317362	1
Ccl2	-0.53724	-0.5574	-0.55771	0.8244	0.82795	1
Ifi44	-0.289258	-0.365568	-0.366748	0.504062	0.517512	1
Mmp9	-0.3114818	-0.4211318	-0.4228318	0.5680602	0.5873852	1
Csf3	-0.377092	-0.377362	-0.377372	0.565888	0.565938	1
Ptgs2	-0.212499	-0.2662361	-0.2670687	0.36816696	0.37763696	1
Ptgs1	-0.0983312	-0.3233112	-0.3267912	0.3543928	0.3940408	1
Limk1	-0.29211	-0.30314	-0.30331	0.44831	0.45025	1
Il6	-0.357284	-0.258174	-0.256644	0.444786	0.427316	1
Ifit2	-0.320816	-0.206366	-0.204596	0.375974	0.355804	1
Nos2	-0.251096	-0.226406	-0.226016	0.353934	0.349584	1
Oasl1	-0.279208	-0.213348	-0.212328	0.358242	0.346642	1
Birc2	0.1202734	0.3099554	0.3128944	-0.3548466	-0.3882766	2
Mef2c	0.277936	0.286706	0.286836	-0.424964	-0.426514	2
Mafg	0.255614	0.268044	0.268244	-0.394856	-0.397046	2
Il6ra	0.31962	0.33162	0.33182	-0.49048	-0.49258	2
Bcl6	0.36892	0.36402	0.36392	-0.54888	-0.54798	2
Tlr9	0.313278	0.339948	0.340358	-0.494442	-0.499142	2
Cd40	0.350673	0.285309	0.284296	-0.465899	-0.454379	2

Figure 6C. Normalized expression levels of significantly differentially expressed genes between the LPS + BBS and LPS + Myco groups. Treatment groups are labeled in the top row, with a number 1-3 denoting the sample. Each gene symbol is further defined in the gene table. Cluster 1 genes experienced higher levels transcription in the presence of LPS and the *Mycobacterium* than in the LPS + BBS group, while cluster 2 genes were more highly expressed in the LPS + BBS group than in the LPS + Myco group.

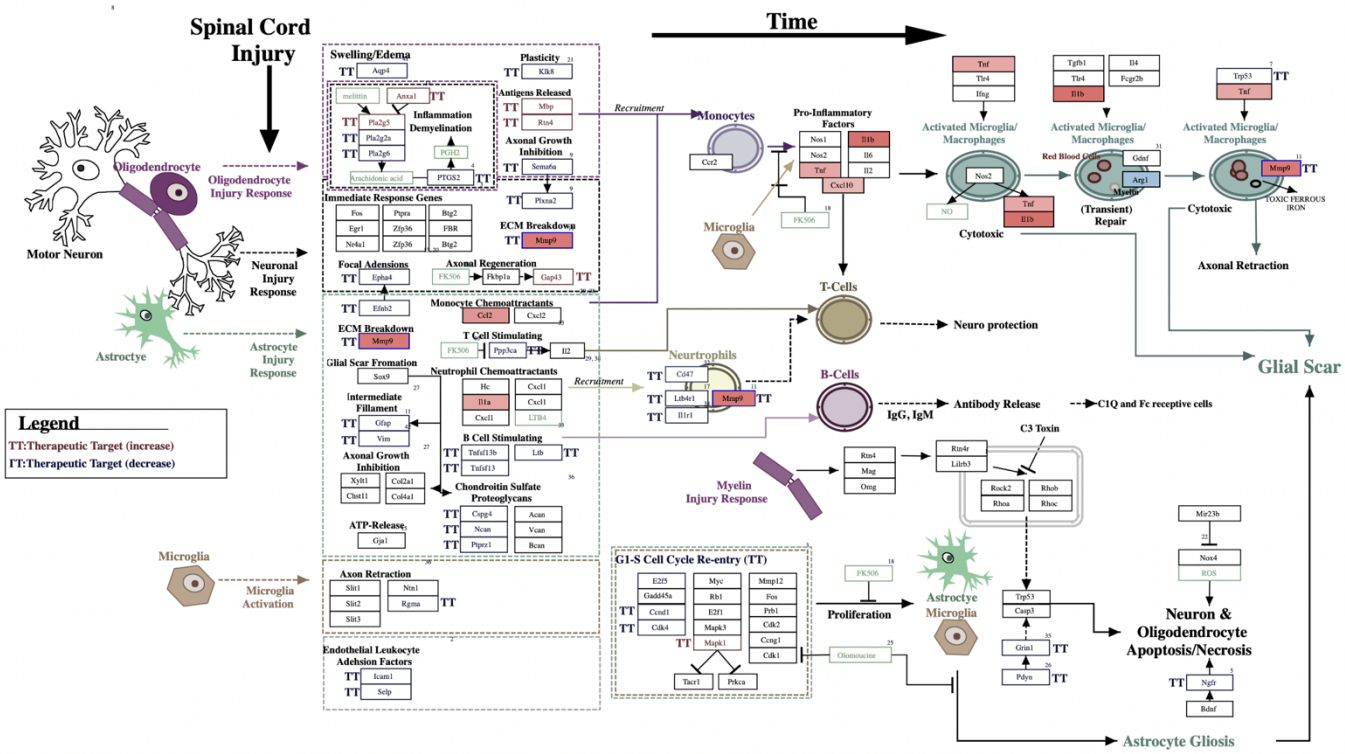

Figure 14B. Diagram of genes and processes activated after spinal cord injury. This pathway diagram shows genes upregulated during the damage response in the spinal cord. Transcription of certain involved genes increased in the Myco group, as denoted by red coloring. Chart taken from Rosalind (https://rosalind.bio/) using data from WikiPathways (Martens et al., 2021).

Works Cited:

Bardina, S. V., Michlmayr, D., Hoffman, K. W., Obara, C. J., Sum, J., Charo, I. F., Lu, W., Pletnev, A. G., & Lim, J. K. (2015). Differential Roles of Chemokines CCL2 and CCL7 in Monocytosis and Leukocyte Migration during West Nile Virus Infection. *The Journal of Immunology*, *195*(9), 4306–4318. https://doi.org/10.4049/jimmunol.1500352

Blasi, E., Barluzzi, R., Bocchini, V., Mazzolla, R., & Bistoni, F. (1990). Immortalization of murine microglial cells by a v-raf / v-myc carrying retrovirus. *Journal of Neuroimmunology*, *27*(2), 229–237. https://doi.org/10.1016/0165-5728(90)90073-V

Böbel, T. S., Hackl, S. B., Langgartner, D., Jarczok, M. N., Rohleder, N., Rook, G. A., Lowry, C. A., Gündel, H., Waller, C., & Reber, S. O. (2018). Less immune activation following social stress in rural vs. Urban participants raised with regular or no animal contact, respectively. *Proceedings of the National Academy of Sciences*, *115*(20), 5259–5264. https://doi.org/10.1073/pnas.1719866115

Boni, F. G., Hamdi, I., Koundi, L. M., Shrestha, K., & Xie, J. (2022). Cytokine storm in tuberculosis and IL-6 involvement. *Infection, Genetics and Evolution*, *97*, 105166. https://doi.org/10.1016/j.meegid.2021.105166

Bourel, J., Planche, V., Dubourdieu, N., Oliveira, A., Séré, A., Ducourneau, E.-G., Tible, M., Maitre, M., Lesté-Lasserre, T., Nadjar, A., Desmedt, A., Ciofi, P., Oliet, S. H., Panatier, A., & Tourdias, T. (2021). Complement C3 mediates early hippocampal neurodegeneration and memory impairment in experimental multiple sclerosis. *Neurobiology of Disease*, *160*, 105533. https://doi.org/10.1016/j.nbd.2021.105533

Cai, W., Dai, X., Chen, J., Zhao, J., Xu, M., Zhang, L., Yang, B., Zhang, W., Rocha, M., Nakao, T., Kofler, J., Shi, Y., Stetler, R. A., Hu, X., & Chen, J. (n.d.). STAT6/Arg1 promotes

microglia/macrophage efferocytosis and inflammation resolution in stroke mice. *JCI Insight*, *4*(20), e131355. https://doi.org/10.1172/jci.insight.131355

Doolittle, R. F. (2011). Coagulation in Vertebrates with a Focus on Evolution and Inflammation. *Journal of Innate Immunity*, *3*(1), 9–16. https://doi.org/10.1159/000321005

DRIESSLER, F., VENSTROM, K., SABAT, R., ASADULLAH, K., & SCHOTTELIUS, A. J. (2004). Molecular mechanisms of interleukin-10-mediated inhibition of NF-κB activity: A role for p50. *Clinical and Experimental Immunology*, *135*(1), 64–73. https://doi.org/10.1111/j.1365-2249.2004.02342.x

Ehlers, S., & Kaufmann, S. H. E. (2010). Infection, inflammation, and chronic diseases: Consequences of a modern lifestyle. *Trends in Immunology*, *31*(5), 184–190. https://doi.org/10.1016/j.it.2010.02.003

Feghali, C. A., & Wright, T. M. (1997). Cytokines in acute and chronic inflammation. *Frontiers in Bioscience-Landmark*, *2*(4), Article 4. https://doi.org/10.2741/A171

Frank, M. G., Barrientos, R. M., Biedenkapp, J. C., Rudy, J. W., Watkins, L. R., & Maier, S. F. (2006). MRNA up-regulation of MHC II and pivotal pro-inflammatory genes in normal brain aging. *Neurobiology of Aging*, *27*(5), 717–722. https://doi.org/10.1016/j.neurobiolaging.2005.03.013

Furman, D., Campisi, J., Verdin, E., Carrera-Bastos, P., Targ, S., Franceschi, C., Ferrucci, L., Gilroy, D. W., Fasano, A., Miller, G. W., Miller, A. H., Mantovani, A., Weyand, C. M., Barzilai, N., Goronzy, J. J., Rando, T. A., Effros, R. B., Lucia, A., Kleinstreuer, N., & Slavich, G. M. (2019). Chronic inflammation in the etiology of disease across the life span. *Nature Medicine*, *25*(12), Article 12. https://doi.org/10.1038/s41591-019-0675-0

Garner, K. M., Amin, R., Johnson, R. W., Scarlett, E. J., & Burton, M. D. (2018). Microglia priming by interleukin-6 signaling is enhanced in aged mice. *Journal of Neuroimmunology*, *324*, 90–99. https://doi.org/10.1016/j.jneuroim.2018.09.002

Geisbrecht, B. V., Lambris, J. D., & Gros, P. (2022). Complement component C3: A structural perspective and potential therapeutic implications. *Seminars in Immunology*, *59*, 101627. https://doi.org/10.1016/j.smim.2022.101627

Grazia Roncarolo, M., Gregori, S., Battaglia, M., Bacchetta, R., Fleischhauer, K., & Levings, M. K. (2006). Interleukin-10-secreting type 1 regulatory T cells in rodents and humans. *Immunological Reviews*, *212*(1), 28–50. https://doi.org/10.1111/j.0105-2896.2006.00420.x

Henn, A. (2009). The suitability of BV2 cells as alternative model system for primary microglia cultures or for animal experiments examining brain inflammation. *ALTEX*, 83–94. https://doi.org/10.14573/altex.2009.2.83

Hoebe, K., Janssen, E., & Beutler, B. (2004). The interface between innate and adaptive immunity. *Nature Immunology*, *5*(10), Article 10. https://doi.org/10.1038/ni1004-971

Holbrook, E. M., Zambrano, C. A., Wright, C. T. O., Dubé, E. M., Stewart, J. R., Sanders, W. J., Frank, M. G., MacDonald, A. S., Reber, S. O., & Lowry, C. A. (2023). Mycobacterium vaccae NCTC 11659, a Soil-Derived Bacterium with Stress Resilience Properties, Modulates the Proinflammatory Effects of LPS in Macrophages. *International Journal of Molecular Sciences*, *24*(6), Article 6. https://doi.org/10.3390/ijms24065176

Józefowski, S., Sobota, A., & Kwiatkowska, K. (2008). How Mycobacterium tuberculosis subverts host immune responses. *BioEssays*, *30*(10), 943–954. https://doi.org/10.1002/bies.20815

Kany, S., Vollrath, J. T., & Relja, B. (2019). Cytokines in Inflammatory Disease. *International Journal of Molecular Sciences*, *20*(23), Article 23. https://doi.org/10.3390/ijms20236008

Lawson, L. J., Perry, V. H., Dri, P., & Gordon, S. (1990). Heterogeneity in the distribution and morphology of microglia in the normal adult mouse brain. *Neuroscience*, *39*(1), 151–170. https://doi.org/10.1016/0306-4522(90)90229-W

Liu, L., Jiang, Y., & Steinle, J. J. (2022). TNFAIP3 is anti-inflammatory in the retinal vasculature. *Molecular Vision*, *28*, 124–129.

Loane, D. J., & Byrnes, K. R. (2010). Role of Microglia in Neurotrauma. *Neurotherapeutics*, *7*(4), 366–377. https://doi.org/10.1016/j.nurt.2010.07.002

Martens, M., Ammar, A., Riutta, A., Waagmeester, A., Slenter, D. N., Hanspers, K., A. Miller, R., Digles, D., Lopes, E. N., Ehrhart, F., Dupuis, L. J., Winckers, L. A., Coort, S. L., Willighagen, E. L., Evelo, C. T., Pico, A. R., & Kutmon, M. (2021). WikiPathways: Connecting communities. *Nucleic Acids Research*, *49*(D1), D613–D621. https://doi.org/10.1093/nar/gkaa1024

Mercuri, E., Atkinson, J., Braddick, O., Anker, S., Cowan, F., Rutherford, M., Pennock, J., & Dubowitz, L. (1997). Basal ganglia damage and impaired visual function in the newborn infant. *Archives of Disease in Childhood - Fetal and Neonatal Edition*, *77*(2), F111–F114. https://doi.org/10.1136/fn.77.2.F111

NCounter® Sprint Profiler. (n.d.). NanoString. Retrieved April 2, 2023, from https://nanostring.com/products/ncounter-analysis-system/sprint-profiler/

Ouabbou, S., He, Y., Butler, K., & Tsuang, M. (2020). Inflammation in Mental Disorders: Is the Microbiota the Missing Link? *Neuroscience Bulletin*, *36*(9), 1071–1084. https://doi.org/10.1007/s12264-020-00535-1

Pace, T. W. W., Mletzko, T. C., Alagbe, O., Musselman, D. L., Nemeroff, C. B., Miller, A. H., & Heim, C. M. (2006). Increased Stress-Induced Inflammatory Responses in Male Patients With Major Depression and Increased Early Life Stress. *American Journal of Psychiatry*, *163*(9), 1630–1633. https://doi.org/10.1176/ajp.2006.163.9.1630

Queen, A. E., Moerdyk-Schauwecker, M., McKee, L. M., Leamy, L. J., & Huet, Y. M. (2016). Differential Expression of Inflammatory Cytokines and Stress Genes in Male and Female Mice in Response to a Lipopolysaccharide Challenge. *PLOS ONE*, *11*(4), e0152289. https://doi.org/10.1371/journal.pone.0152289

Reber, S. O., Siebler, P. H., Donner, N. C., Morton, J. T., Smith, D. G., Kopelman, J. M., Lowe, K. R., Wheeler, K. J., Fox, J. H., Hassell, J. E., Greenwood, B. N., Jansch, C., Lechner, A., Schmidt, D., Uschold-Schmidt, N., Füchsl, A. M., Langgartner, D., Walker, F. R., Hale, M. W., … Lowry, C. A. (2016). Immunization with a heat-killed preparation of the environmental bacterium Mycobacterium vaccae promotes stress resilience in mice. *Proceedings of the National Academy of Sciences*, *113*(22), E3130–E3139. https://doi.org/10.1073/pnas.1600324113

Ritchie, M. E., Phipson, B., Wu, D., Hu, Y., Law, C. W., Shi, W., & Smyth, G. K. (2015). Limma powers differential expression analyses for RNA-sequencing and microarray studies. *Nucleic Acids Research*, *43*(7), e47. https://doi.org/10.1093/nar/gkv007

Rook, G. A. W., Lowry, C. A., & Raison, C. L. (2013). Microbial 'Old Friends', immunoregulation and stress resilience. *Evolution, Medicine, and Public Health*, *2013*(1), 46–64. https://doi.org/10.1093/emph/eot004

Schetters, S. T. T., Gomez-Nicola, D., Garcia-Vallejo, J. J., & Van Kooyk, Y. (2018). Neuroinflammation: Microglia and T Cells Get Ready to Tango. *Frontiers in Immunology*, *8*. https://www.frontiersin.org/articles/10.3389/fimmu.2017.01905

Sweeney, K. A., Dao, D. N., Goldberg, M. F., Hsu, T., Venkataswamy, M. M., Henao-Tamayo, M., Ordway, D., Sellers, R. S., Jain, P., Chen, B., Chen, M., Kim, J., Lukose, R., Chan, J., Orme, I. M., Porcelli, S. A., & Jacobs, W. R. (2011). A recombinant Mycobacterium smegmatis induces potent bactericidal immunity against Mycobacterium tuberculosis. *Nature Medicine*, *17*(10), Article 10. https://doi.org/10.1038/nm.2420

Wallace, R. J., Jr., Nash, D. R., Tsukamura, M., Blacklock, Z. M., & Silcox, V. A. (1988). Human Disease Due to Mycobacterium smegmatis. *The Journal of Infectious Diseases*, *158*(1), 52–59. https://doi.org/10.1093/infdis/158.1.52

Zuany-Amorim, C., Sawicka, E., Manlius, C., Le Moine, A., Brunet, L. R., Kemeny, D. M., Bowen, G., Rook, G., & Walker, C. (2002). Suppression of airway eosinophilia by killed Mycobacterium vaccae-induced allergen-specific regulatory T-cells. *Nature Medicine*, *8*(6), Article 6. https://doi.org/10.1038/nm0602-625

Gene List, nCounter Mouse Inflammation v2 Panel
(Cat. No. XT-CSO-MIN2-12; NanoString Seattle, WA)

Name	Gene ID	Alias	Description
Cfd	11537	Adn|DF	complement factor D (adipsin)
Ager	11596	RAGE	advanced glycosylation end product-specific receptor
Alox12	11684	9930022G08	arachidonate 12-lipoxygenase
Alox15	11687	12-LO|12/15	arachidonate 15-lipoxygenase
Alox5	11689	5-LO|5-LOX|	arachidonate 5-lipoxygenase
Birc2	11797	AW146227|A	baculoviral IAP repeat-containing 2
Areg	11839	AR|Mcub|Sc	amphiregulin
Arg1	11846	AI|AI256583	arginase, liver
Rhoa	11848	Arha|Arha1|	ras homolog gene family, member A
Atf2	11909	Atf-2|CRE-B	activating transcription factor 2
Fxyd2	11936	Atp1g1	FXYD domain-containing ion transport regulator 2
Bcl2l1	12048	Bcl(X)L|Bcl-X	BCL2-like 1
Bcl6	12053	Bcl5	B cell leukemia/lymphoma 6
C1qa	12259	AI255395|C1	complement component 1, q subcomponent, alpha polypeptide
C1qb	12260	-	complement component 1, q subcomponent, beta polypeptide
C2	12263	-	complement component 2 (within H-2S)
C3	12266	AI255234|AS	complement component 3
C3ar1	12267	AZ3B|C3AR|	complement component 3a receptor 1
C6	12274	AW111623	complement component 6

C9	12279	-	complement component 9
Cd4	12504	L3T4|Ly-4	CD4 antigen
Cd86	12524	B7|B7-2|B7	CD86 antigen
Cdc42	12540	AI747189|AU	cell division cycle 42
Cebpb	12608	C/EBPbeta|C	CCAAT/enhancer binding protein (C/EBP), beta
Cfl1	12631	AA959946|C	cofilin 1, non-muscle
Chil3	12655	AI505981|Ch	chitinase-like 3
Cxcr2	12765	CD128|CDw1	chemokine (C-X-C motif) receptor 2
Cxcr4	12767	CD184|Cmka	chemokine (C-X-C motif) receptor 4
Ccr1	12768	Cmkbr1|Mip	chemokine (C-C motif) receptor 1
Ccr3	12771	CC-CKR3|CKR	chemokine (C-C motif) receptor 3
Ccr2	12772	Cc-ckr-2|Ccr2	chemokine (C-C motif) receptor 2
Ccr4	12773	C-C CKR-4|CI	chemokine (C-C motif) receptor 4
Ccr7	12775	CC-CKR-7|CC	chemokine (C-C motif) receptor 7
Creb1	12912	2310001E10I	cAMP responsive element binding protein 1
Crp	12944	AI255847	C-reactive protein, pentraxin-related
Csf1	12977	C87615|Csfn	colony stimulating factor 1 (macrophage)
Csf2	12981	Csfgm|GMC	colony stimulating factor 2 (granulocyte-macrophage)
Csf3	12985	Csfg|G-CSF|	colony stimulating factor 3 (granulocyte)
Cd55	13136	Daf|Daf-GPI	CD55 molecule, decay accelerating factor for complement

Daxx	13163	-	Fas death domain-associated protein
Ddit3	13198	CHOP-10|CH	DNA-damage inducible transcript 3
Defa-rs1	13218	2010300L12F	defensin, alpha, related sequence 1
Twist2	13345	Dermo1|bHL	twist basic helix-loop-helix transcription factor 2
Elk1	13712	Elk-1	ELK1, member of ETS oncogene family
Ptk2	14083	FAK|FRNK|F	PTK2 protein tyrosine kinase 2
Fasl	14103	APT1LG1|CD	Fas ligand (TNF superfamily, member 6)
Flt1	14254	AI323757|Fl	FMS-like tyrosine kinase 1
Fos	14281	D12Rfj1|c-fc	FBJ osteosarcoma oncogene
Gnaq	14682	1110005L02F	guanine nucleotide binding protein, alpha q polypeptide
Gnas	14683	5530400H20	GNAS (guanine nucleotide binding protein, alpha stimulating) complex locus
Gnb1	14688	AA409223|C	guanine nucleotide binding protein (G protein), beta 1
Gngt1	14699	G(y)1|Gng1	guanine nucleotide binding protein (G protein), gamma transducing activity po
Grb2	14784	AA408164|A	growth factor receptor bound protein 2
Nr3c1	14815	GR|Grl-1|Gr	nuclear receptor subfamily 3, group C, member 1
Cxcl1	14825	Fsp|Gro1|KC	chemokine (C-X-C motif) ligand 1
Cfb	14962	AI195813|AI	complement factor B
H2-Eb1	14969	Eb|H-2Eb|H2	histocompatibility 2, class II antigen E beta
Hc	15139	C5|C5a|He	hemolytic complement
Hif1a	15251	AA959795|H	hypoxia inducible factor 1, alpha subunit
Hmgb1	15289	HMG-1|Hmg	high mobility group box 1
Hmgn1	15312	HMG-14|Hm	high mobility group nucleosomal binding domain 1
Hras	15461	H-ras|Ha-ras	Harvey rat sarcoma virus oncogene
Hspb1	15507	27kDa|Hsp25	heat shock protein 1
Cxcl10	15945	C7|CRG-2|IN	chemokine (C-X-C motif) ligand 10
Ifit1	15957	ISG56|Ifi56|	interferon-induced protein with tetratricopeptide repeats 1
Ifit2	15958	AV302338|If	interferon-induced protein with tetratricopeptide repeats 2
Ifit3	15959	Ifi49|P49	interferon-induced protein with tetratricopeptide repeats 3
Ifna1	15962	Ifa1	interferon alpha 1
Ifnb1	15977	IFN-beta|IFN	interferon beta 1, fibroblast
Ifng	15978	IFN-g|Ifg	interferon gamma
Il10	16153	CSIF|Il-10	interleukin 10
Il10rb	16155	6620401D04	interleukin 10 receptor, beta
Il11	16156	IL-11	interleukin 11
Il12a	16159	IL-12p35|Il-1	interleukin 12a
Il12b	16160	Il-12b|Il-12p	interleukin 12b
Il13	16163	Il-13	interleukin 13
Il15	16168	AI503618|IL-	interleukin 15
Il17a	16171	Ctla-8|Ctla8	interleukin 17A
Il18	16173	Igif|Il-18	interleukin 18
Il18rap	16174	AcPL|IL-18R-	interleukin 18 receptor accessory protein
Il1a	16175	Il-1a	interleukin 1 alpha
Il1b	16176	IL-1beta|Il-1	interleukin 1 beta
Il1r1	16177	CD121a|CD1	interleukin 1 receptor, type I
Il1rap	16180	6430709H04	interleukin 1 receptor accessory protein
Il1rn	16181	F630041P17I	interleukin 1 receptor antagonist
Il2	16183	Il-2	interleukin 2
Il3	16187	BPA|Csfmu|	interleukin 3
Il4	16189	BSF-1|Il-4	interleukin 4
Il5	16191	Il-5	interleukin 5

Il6	16193	Il-6	interleukin 6
Il6ra	16194	CD126|IL-6R	interleukin 6 receptor, alpha
Il7	16196	A630026I06F	interleukin 7
Il9	16198	Il-9|P40	interleukin 9
Irf1	16362	AU020929|I	interferon regulatory factor 1
Itgb2	16414	2E6|AI52852	integrin beta 2
Jun	16476	AP-1|Junc|c	jun proto-oncogene
Kng1	16644	Kng	kininogen 1
Limk1	16885	KIZ-1|LIMK-	LIM-domain containing, protein kinase
Lta	16992	LT|LT-[a]|LT	lymphotoxin A
Ltb	16994	AI662801|LT	lymphotoxin B
Ltb4r1	16995	BLT1|BLTR|	leukotriene B4 receptor 1
Ly96	17087	ESOP-1|MD-	lymphocyte antigen 96
Smad7	17131	Madh7	SMAD family member 7
Maff	17133	-	v-maf musculoaponeurotic fibrosarcoma oncogene family, protein F (avian)
Mafg	17134	AA545192|C	v-maf musculoaponeurotic fibrosarcoma oncogene family, protein G (avian)
Mafk	17135	AW061068|I	v-maf musculoaponeurotic fibrosarcoma oncogene family, protein K (avian)
Mapkapk2	17164	AA960234|M	MAP kinase-activated protein kinase 2
Mapkapk5	17165	MK5|PRAK	MAP kinase-activated protein kinase 5
Masp1	17174	AW048060|(	mannan-binding lectin serine peptidase 1
Masp2	17175	MASP-2|MA	mannan-binding lectin serine peptidase 2
Max	17187	AA960152|A	Max protein
Mbl2	17195	L-MBP|MBL	mannose-binding lectin (protein C) 2
Mef2a	17258	A430079H05	myocyte enhancer factor 2A
Mef2b	17259	AI451606	myocyte enhancer factor 2B
Mef2c	17260	5430401D19	myocyte enhancer factor 2C
Mef2d	17261	C80750	myocyte enhancer factor 2D
Cxcl9	17329	BB139920|C	chemokine (C-X-C motif) ligand 9
Mknk1	17346	2410048M24	MAP kinase-interacting serine/threonine kinase 1
Mmp3	17392	EMS-2|MMP	matrix metallopeptidase 3
Mmp9	17395	AW743869|I	matrix metallopeptidase 9
Mrc1	17533	AW259686|(	mannose receptor, C type 1
Mx1	17857	AI893580|M	MX dynamin-like GTPase 1
Mx2	17858	AI528743|M	MX dynamin-like GTPase 2
Myc	17869	AU016757|M	myelocytomatosis oncogene
Myd88	17874	-	myeloid differentiation primary response gene 88
Myl2	17906	MLC-2|MLC-	myosin, light polypeptide 2, regulatory, cardiac, slow
Nfatc3	18021	C80703|D8E	nuclear factor of activated T cells, cytoplasmic, calcineurin dependent 3
Nfe2l2	18024	Nrf2	nuclear factor, erythroid derived 2, like 2
Nfkb1	18033	NF-KB1|NF-	nuclear factor of kappa light polypeptide gene enhancer in B cells 1, p105
Nos2	18126	MAC-NOS|N	nitric oxide synthase 2, inducible
Pdgfa	18590	-	platelet derived growth factor, alpha
Pik3c2g	18705	C80387|PI3K	phosphatidylinositol 3-kinase, C2 domain containing, gamma polypeptide
Prkca	18750	AI875142|Pk	protein kinase C, alpha
Prkcb	18751	A130082F03	protein kinase C, beta
Pla2g4a	18783	Pla2g4|cPLA	phospholipase A2, group IVA (cytosolic, calcium-dependent)
Plcb1	18795	3110043I21R	phospholipase C, beta 1
Ccl21a	18829	6CKBAC2|6C	chemokine (C-C motif) ligand 21A (serine)
Ptger1	19216	42kDa|EP1|I	prostaglandin E receptor 1 (subtype EP1)
Ptger2	19217	EP2|Ptgerep	prostaglandin E receptor 2 (subtype EP2)

Ptger3	19218	EP3|Pgerep3	prostaglandin E receptor 3 (subtype EP3)
Ptger4	19219	EP4|Ptgerep	prostaglandin E receptor 4 (subtype EP4)
Ptgfr	19220	AI957154|PC	prostaglandin F receptor
Ptgir	19222	IP|PGI2	prostaglandin I receptor (IP)
Ptgs1	19224	COX1|Cox-1|	prostaglandin-endoperoxide synthase 1
Ptgs2	19225	COX2|Cox-2|	prostaglandin-endoperoxide synthase 2
Rac1	19353	AL023026|D	RAS-related C3 botulinum substrate 1
Rela	19697	p65	v-rel reticuloendotheliosis viral oncogene homolog A (avian)
Relb	19698	shep	avian reticuloendotheliosis viral (v-rel) oncogene related B
Ripk1	19766	D330015H01	receptor (TNFRSF)-interacting serine-threonine kinase 1
Rock2	19878	B230113H15	Rho-associated coiled-coil containing protein kinase 2
Ccl11	20292	Scya11|eota	chemokine (C-C motif) ligand 11
Ccl17	20295	Abcd-2|Scya	chemokine (C-C motif) ligand 17
Ccl2	20296	AI323594|H(	chemokine (C-C motif) ligand 2
Ccl20	20297	CKb4|LARC|	chemokine (C-C motif) ligand 20
Ccl22	20299	ABCD-1|DCB	chemokine (C-C motif) ligand 22
Ccl3	20302	AI323804|G(	chemokine (C-C motif) ligand 3
Ccl4	20303	AT744.1|Act	chemokine (C-C motif) ligand 4
Ccl5	20304	MuRantes|R	chemokine (C-C motif) ligand 5
Ccl7	20306	MCP-3|Scya	chemokine (C-C motif) ligand 7
Ccl8	20307	1810063B20	chemokine (C-C motif) ligand 8
Cxcl2	20310	CINC-2a|GR(	chemokine (C-X-C motif) ligand 2
Cxcl5	20311	AMCF-II|ENA	chemokine (C-X-C motif) ligand 5
Shc1	20416	Shc|ShcA|p(	src homology 2 domain-containing transforming protein C1
Stat1	20846	2010005J02F	signal transducer and activator of transcription 1
Stat2	20847	1600010G07	signal transducer and activator of transcription 2
Stat3	20848	1110034C02I	signal transducer and activator of transcription 3
Tbxa2r	21390	TP|TXA2-R	thromboxane A2 receptor
Tcf4	21413	5730422P05I	transcription factor 4
Tgfb1	21803	TGF-beta1|T	transforming growth factor, beta 1
Tgfb2	21808	BB105277|T	transforming growth factor, beta 2
Tgfb3	21809	TGF-beta-3|	transforming growth factor, beta 3
Tgfbr1	21812	ALK5|AU017	transforming growth factor, beta receptor I
Tlr1	21897	-	toll-like receptor 1
Tlr4	21898	Lps|Ly87|Ra	toll-like receptor 4
Tlr6	21899	-	toll-like receptor 6
Tnf	21926	DIF|TNF-a|T	tumor necrosis factor
Tnfaip3	21929	A20|Tnfip3	tumor necrosis factor, alpha-induced protein 3
Cd40	21939	AI326936|Bp	CD40 antigen
Cd40lg	21947	CD154|CD40	CD40 ligand
Traf2	22030	AI325259	TNF receptor-associated factor 2
Tyrobp	22177	DAP12|KARA	TYRO protein tyrosine kinase binding protein
Ccl19	24047	CKb11|ELC|M	chemokine (C-C motif) ligand 19
Tlr2	24088	Ly105	toll-like receptor 2
Map2k1	26395	MAPKK1|ME	mitogen-activated protein kinase kinase 1
Map2k4	26398	JNKK1|MEK4	mitogen-activated protein kinase kinase 4
Map2k6	26399	MEK6|MKK6	mitogen-activated protein kinase kinase 6
Map3k1	26401	MAPKKK1|M	mitogen-activated protein kinase kinase kinase 1
Map3k5	26408	7420452D20	mitogen-activated protein kinase kinase kinase 5
Map3k7	26409	B430101B05	mitogen-activated protein kinase kinase kinase 7

Mapk1	26413	9030612K14	mitogen-activated protein kinase 1
Mapk14	26416	CSBP2|Crk1|	mitogen-activated protein kinase 14
Mapk3	26417	Erk-1|Erk1|E	mitogen-activated protein kinase 3
Mapk8	26419	AI849689|JN	mitogen-activated protein kinase 8
Irf5	27056	AW491843|I	interferon regulatory factor 5
Keap1	50868	INRF2|mKIA	kelch-like ECH-associated protein 1
C1s1	50908	AA959438|A	complement component 1, s subcomponent 1
C1ra	50909	AI132558|C1	complement component 1, r subcomponent A
Il22	50929	IL-22|IL-22a	interleukin 22
Tnfsf14	50930	HVEM-L|HVE	tumor necrosis factor (ligand) superfamily, member 14
Tslp	53603	-	thymic stromal lymphopoietin
Tlr5	53791	-	toll-like receptor 5
Irf7	54123	-	interferon regulatory factor 7
Irf3	54131	C920001K05I	interferon regulatory factor 3
Tollip	54473	4930403G24	toll interacting protein
Ccl24	56221	CKb-6|MPIF-	chemokine (C-C motif) ligand 24
Ltb4r2	57260	5830462O07	leukotriene B4 receptor 2
Retnla	57262	1810019L16F	resistin like alpha
Cysltr1	58861	BB147369|C	cysteinyl leukotriene receptor 1
Iigp1	60440	2900074L10F	interferon inducible GTPase 1
Il21	60505	IL-21	interleukin 21
Hspb2	69253	27kDa|2810(	heat shock protein 2
Cysltr2	70086	2300001H05	cysteinyl leukotriene receptor 2
Tradd	71609	9130005N23	TNFRSF1A-associated via death domain
Rps6ka5	73086	3110005L17F	ribosomal protein S6 kinase, polypeptide 5
Rapgef2	76089	5830453M24	Rap guanine nucleotide exchange factor (GEF) 2
Ifi27l2a	76933	2310061N23	interferon, alpha-inducible protein 27 like 2A
Tlr9	81897	-	toll-like receptor 9
Il23a	83430	IL-23|p19	interleukin 23, alpha subunit p19
Trem2	83433	TREM-2|Tre	triggering receptor expressed on myeloid cells 2
Cd163	93671	CD163v2|CD	CD163 antigen
Hmgb2	97165	C80539|HM(	high mobility group box 2
Ifi44	99899	A430056A10	interferon-induced protein 44
Nod1	107607	C230079P11	nucleotide-binding oligomerization domain containing 1
C7	109828	A530026G17	complement component 7
Raf1	110157	6430402F14I	v-raf-leukemia viral oncogene 1
C8b	110382	4930439B20	complement component 8, beta polypeptide
Tlr3	142980	AI957183	toll-like receptor 3
Tlr7	170743	-	toll-like receptor 7
Tlr8	170744	-	toll-like receptor 8
Ripk2	192656	2210420D18	receptor (TNFRSF)-interacting serine-threonine kinase 2
Hdac4	208727	4932408F19I	histone deacetylase 4
Hsh2d	209488	ALX|Hsh2	hematopoietic SH2 domain containing
Il23r	209590	IL-23R	interleukin 23 receptor
Nlrp3	216799	AGTAVPRL|A	NLR family, pyrin domain containing 3
Cxcr1	227288	Il8ra	chemokine (C-X-C motif) receptor 1
C8a	230558	-	complement component 8, alpha polypeptide
Oasl1	231655	7530414C13I	2'-5' oligoadenylate synthetase-like 1
Nox1	237038	GP91-2|MO)	NADPH oxidase 1
Il22ra2	237310	CRF2-10|CRI	interleukin 22 receptor, alpha 2
Oas2	246728	Oasl11	2'-5' oligoadenylate synthetase 2
Oas1a	246730	L3	2'-5' oligoadenylate synthetase 1A
Nod2	257632	ACUG|BLAU	nucleotide-binding oligomerization domain containing 2
Ppp1r12b	329251	1810037O03	protein phosphatase 1, regulatory (inhibitor) subunit 12B
Cxcl3	330122	Dcip1|Gm19	chemokine (C-X-C motif) ligand 3
Map3k9	338372	E130314H24	mitogen-activated protein kinase kinase kinase 9
C4a	625018	Slp|SlpA	complement component 4A (Rodgers blood group)
H2-Ea-ps	100504404	AI323765|E-	histocompatibility 2, class II antigen E alpha, pseudogene